

Introduction

David M. Rowe
*University of Wales, Cardiff
U.K.*

In 1823 Seebeck reported the results of experiments in which a compass needle was deflected if placed in the vicinity of a closed loop, formed from two dissimilar conductors, when one of the junctions was heated.¹ Seebeck erroneously concluded that the interaction was a magnetic phenomenon and, in pursuing this line of thought, attempted to relate the Earth's magnetism to the temperature difference between the equator and the Poles. Nevertheless, he did investigate the phenomenon in a large number of materials, including some we now call semiconductors, and arranged them in order of the product $\alpha\sigma$, where α is the Seebeck coefficient and σ the electrical conductivity. The Seebeck coefficient is expressed in volts per degree, or more often in microvolts per degree $\mu\text{V}\text{K}^{-1}$. The Seebeck series formed in this way is very similar to the present-day thermoelectric series and, had Seebeck employed the first and last members of his series in a thermocouple, he could have converted thermal energy into electricity in 1821 with an efficiency of about 3%, which compares very favorably with the most efficient steam engine of the day. With the benefit of hindsight it is apparent from Seebeck's account that the phenomenon observed was caused by an electric current flowing in the circuit and that he had discovered the so-called thermoelectric effects.

Some 12 years later, a complementary effect was discovered by Peltier,² who observed temperature changes in the vicinity of the junction between dissimilar conductors when a current passed. Although Peltier used the Seebeck effect in his experiments as a source of weak currents, he failed to appreciate the fundamental nature of his observations, or to relate the effect to the findings of Seebeck. The true nature of the Peltier effect was explained by Lenz³ in 1838. He concluded that, depending upon the direction of the current flow, heat is absorbed or generated at a junction between two conductors and demonstrated this by freezing water at a bismuth-junction and melting the ice by reversing the direction of current flow.

The lack of interest and slow progress in thermoelectric application which followed the discovery of thermoelectric phenomena are understandable when one recalls that much more exciting discoveries were made during this period. This was the era of electromagnetism, with the initial discoveries of Oersted being followed by investigations of researchers such as Ampere and Laplace and culminating in the formulation of the laws of electromagnetic induction by Faraday.

Thermoelectricity enjoyed a temporary revival from 1850 with the development of thermodynamics when interest focused on all forms of energy conversion. In 1851⁴ W. Thomson (Lord Kelvin) established a relationship between the Seebeck and Peltier coefficients and predicted the existence of a third thermoelectric effect, the Thomson effect, which he subsequently observed experimentally. This effect relates to the heating or cooling in a single homogeneous conductor when a current passes along it in the presence of a temperature gradient.

The possibility of using thermoelectric phenomena in the generation of electricity was considered in 1885 by Rayleigh who first calculated, although incorrectly, the efficiency of a thermoelectric generator. In 1909⁵ and 1911⁶ Alenkirch gave a satisfactory theory of thermoelectric generation and refrigeration and showed that good thermoelectric materials should possess large

Serbeck coefficients with low thermal conductivity (k) to retain the heat at the junction and low electrical resistance to minimize Joule heating. These desirable properties were embodied in a so-called figure-of-merit Z , where $Z = q^2T/k$ and the unit of Z is MK. At a given absolute temperature T , since Z may vary with T , a useful nondimensional figure-of-merit is zT .

Although the properties favorable for thermoelectric applications were well known, the important advantages offered by Serbeck's mineral semiconductors were overlooked with the attention of researchers focused on metal and metal alloys. In these materials the ratio of the thermal conductivity to electrical conductivity is a constant (Wiedemann-Franz-Lorenz law) and it is not possible to reduce one while increasing the other. Consequently, the metals best suited are those with the highest Seebeck coefficients. Most metals possess Seebeck coefficients of 10 μVK^{-1} or less, giving associated generating efficiencies of a fraction of 1%, which are uneconomical as a source of electrical power. Similar considerations also led to the conclusion that thermoelectric refrigeration was an uneconomic proposition.

Renewed interest in thermoelectricity accompanied the development in the late 1930s of synthetic semiconductors that possessed Seebeck coefficients in excess of 100 μVK^{-1} and in 1947 Teltex² constructed a generator that operated with an efficiency of about 5%. In 1949 Ioffe³ developed a theory of semiconductor thermoelements and in 1954 Goldberid and Douglas demonstrated that cooling from ordinary ambient temperatures down to below 0°C was possible.⁴ Unfortunately, in semiconductors the ratio of the thermal to electrical conductivity is greater than in metals owing to their poorer electrical conductivity. It was not obvious that semiconductors were superior thermoelectric materials and, apart from the Soviet activities, interest again waned. Research into compound semiconductors for possible transistor application in the 1950s resulted in new materials with substantially improved thermoelectric properties and in 1956 Ioffe and his co-workers⁵ demonstrated that the ratio could be decreased if the thermoelectric material is alloyed with an isomorphous element or compound. Spurred on by possible military applications a tremendous variety of materials was undertaken, particularly at the RCA Laboratories in the U.S., which resulted in the discovery of a few semiconductors with zT approaching 1.5.

A "modern" thermoelectric converter consists, in essence, of a number of alternate ingot-shaped n- and p-type semiconductor thermoelements, which are connected electrically in series with metal connecting strips sandwiched between two electrically insulating but thermally conducting ceramic plates to form a module. Provided a temperature difference is maintained across the module, electrical power will be delivered to an external load and the device operates as a generator. Conversely, when an electric current is passed through the module, heat is absorbed at one face of the module, rejected at the other face, and the device operates as a refrigerator.

In a thermoelectric generator the efficiency of conversion of heat into electricity depends upon the temperature difference ΔT over which the device operates, on its average temperature of operation, T , and on the performance of the thermoelectric material through its figure-of-merit. The figure-of-merit also determines both the maximum temperature depression and the maximum coefficient of performance of a thermoelectric refrigerator. Consequently, materials that possess large Z values over the intended temperature range of operation are desirable in both generation and refrigeration.

Established thermoelectric materials conveniently fall into three categories depending upon their temperature range of operation. Bismuth telluride and its alloys have the highest figures-of-merit, are extensively employed in refrigeration, and have a maximum operating temperature of around 450 K. Alloys based on lead telluride have the next highest figures-of-merit with silicon germanium alloys having the lowest. Lead telluride and silicon germanium are used in generator applications with upper operating temperatures of around 1000 and 1300 K, respectively.

In the early 1960s a requirement for autonomous sources of electrical power arose from the exploration of space, advances in medical physics, and the exploitation of the Earth's resources in increasingly hostile and inaccessible locations.⁶ Thermoelectric generators are ideally suited to such applications, where their reliability, absence of moving parts, and silent operation outweigh their relatively high cost and low efficiency (typically less than 5%). Advantage can be taken of the simplicity and ruggedness of thermoelectric generators compared with thermomechanical conversion devices.⁷

In situations where periodic refueling is possible and oxygen available, fossil fuel is employed as a heat source. Hydrocarbon fuel has an energy density some 50 times that of a chemical battery and so, provided that the conversion efficiency is better than 2%, a hydrocarbon-fueled system can provide a much lighter and less bulky source of long-term electrical energy than batteries. When annual refueling is not possible, or oxygen is not available, radioactive isotopes serve as heat sources, enabling the generators, which are referred to as radioisotope thermoelectric generators or RTGs, to operate unattended for extended periods; in some instances, such as the Voyager spacecraf

ts launched in 1977, for longer than 17 years.¹¹ Following the fivefold increase in the price of crude oil in 1974, a closer look was taken at the possibility of large-scale production of electricity by the thermoelectric effect. Apart from an abundant supply of easily utilized heat, it was concluded that the economic large-scale thermoelectric generation of electricity would require the cheap production of substantial amounts of semiconductor material, accompanied by a significant improvement in the material figure-of-merit. However, concern over the depletion of the ozone layer in the late 1980s and a general public interest in environmentally friendly energy sources have been accompanied by a renewed interest in thermoelectric generation as a potential source of large-scale electrical power using waste heat.^{14,15}

Thermoelectric cooling has also enjoyed success in domestic food refrigerators, air conditioning, and numerous novel applications where the facility to vary the cooling capacity of the device to match the particular application has proved an important factor.¹⁶ Although large-scale thermoelectric cooling is unlikely ever to match the performance of fricon systems, in some applications its modularity and reliability does offer certain advantages.¹⁷ Significant advances have also been made in the miniaturization of thermoelectric devices, particularly in the development of miniature detectors and sensors^{18,19} and power sources.²⁰

In recent years multistage thermoelectric cooling modules have been developed with as many as six stages enabling temperatures of below 170 K to be achieved with commercial devices.²¹ However, the figure-of-merit of bismuth telluride-based alloys decreases with a reduction in temperature and renewed interest has been shown in materials such as the bismuth-antimony alloys whose thermoelectric performance can be improved by the application of a magnetic field.²² Another magnetic phenomenon, "the Ettingshausen effect", has also proved to be an efficient refrigeration process at low temperatures.²³

Thermoelectric cooling below 150 K has been constrained by the nonavailability of material with a reasonable figure-of-merit at these temperatures apart from n-type bismuth antimonide. The possibility of using a high T_c superconductor (HTSC) as a passive thermoelement was first explored by Goldsmid et al.²⁴ and successfully demonstrated a couple of years later.^{25,26}

Successful commercial exploitation of thermoelectric devices depends to a large degree on increasing the material's figure-of-merit. This in turn is closely dependent upon the formulation of an adequate theoretical model. Solid-state theory has greatly assisted in this direction. Although the models available are, at best, rough approximations of the actual materials, they do provide a useful insight into the desirable basic properties of materials for refrigeration and generation. Models have been developed for all three of the established families of thermoelectric materials.²⁷⁻²⁹ In recent years the upper limit to figure-of-merit has been reinvestigated,³⁰ but realization of the same in practice depends upon many factors, not the least of which is whether or not the material can be prepared.

It is in high-temperature thermoelectric generation that the vast majority of basic research effort is being concentrated with a view to increasing the material figure-of-merit and the device's upper operating temperature. Materials under development are based on the lanthanum chalcogenides and boron-carbon compounds.³¹ Attempts to improve the performance of materials based upon silicon germanium alloys continues. The major effort, which was initially directed at reducing the lattice thermal conductivity by introducing additional disorder into the alloy structure,³²⁻³⁶ is being shifted to improving the electrical power factor.³⁷

Further research into, and development of, thermoelectrics is assured with the continuation of a number of U.S. space projects. In addition, the increased Japanese interest and involvement across the whole spectrum of thermoelectric activities is a pointer to a future increase in the commercial exploitation of this unique energy conversion phenomenon.

References

- Sorbeck, T. J., Magnetic polarization of metals and minerals, *Abhandlungen der Deutschen Akademie der Wissenschaften zu Berlin*, 265, 1822-1823.
- Peltier, J. C., Nouvelles expériences sur la calorité des courants électriques, *Ann. Chim.*, LVI 371, 1834.
- Ioffe, A. F., *Semiconductor Thermoelectric and Thermoelectric Cooling*, Infotech, London, 1957.
- Thomson, W., On a mechanical theory of thermoelectric currents, *Proceedings of the Royal Society of Edinburgh*, 91, 1851.
- Alexenich, E., Über den Nutzefaktor der Thermosäule, *Physikalische Zeitschrift*, 10, 560, 1909.
- Alexenich, E., Electrothermische Kälterezeugung und Reversible Electriche Heizung, *Physikalische Zeitschrift*, 12, 938, 1911.
- Telka, M., The efficiency of thermoelectric generation, *Int. J. Appl. Phys.*, 18, 1136, 1947.
- Ioffe, A. F., *Energeticheskie zasoby termoeklektricheskikh baterii iz poluprovodnikov*, Academy of Sciences of the USSR, Moscow, 1949.
- Goldsmid, H. J. and Douglas, R. W., The use of semiconductors in thermoelectric refrigeration, *Br. J. Appl. Phys.*, 5 (11), 386, 1954.
- Ioffe, A. F., Arayipyan, S. V., Ioffe, A. V., Kolomoets, N. V., and Stibans, L. S., On increasing the efficiency of semiconducting thermocouples, *Dokl. Akad. Nauk SSSR*, 106, 931, 1956.
- Rose, D. M. and Bhundari, C. M., *Modern Thermoelectrics*, Holt Technology, 1983.
- Cooke-Yarborough, E. H. and Yeats, F. W., Efficient thermo-mechanical generation of electricity from the heat of radionuclides, *Proc. XVII BEEC*, August 1975, 1033.
- Rose, D. M., United States thermoelectric activities in space, *Proc. VIIth Int. Conf. Thermoelectric Energy Conversion*, Scherer, S. and Scherer, H., Eds., July 10-13, 1989, Nancy, France, 133.
- Rose, D. M., Thermoelectric generation, *Watt Report*, 1992, Cook, A. W., Ed., 28th Consultative Conference, no. published on behalf of the U.K. Watt Committee on Energy by IEE, 1993.
- Matsuura, K., Rose, D. M., Koimoto, K., Mitani, G., and Tsuyoshi, A., Design Optimisation for a Large Scale Low Temperature Thermoelectric Generator, *Proc. Xth International Conference on Thermoelectrics*, University of Texas at Arlington, October 7-9, 1992, 10.
- Goldsmid, H. J., *Application of Thermoelectricity*, Methuen Monograph, Woensop, B. L., Ed., 1960.
- Blankenship, W. P., Rose, C. M., and Zemanick, P. F., Applications of Thermoelectric Technology to Naval Submarine Cooling, *Proc. VIIIth Int. Conf. Thermoelectric Energy Conversion*, Scherer, S. and Scherer, H., Eds., July 10-13, 1988, Nancy, France, 224.
- Anatychuk, L. I., Moldavsky, M. S., Rasinik, V. V., and Tsyplko, N. K., Thermoelectric batteries for parameters, *Proc. Xth Int. Conf. Thermoelectrics*, Rose, D. M., Ed., Cardiff, Wales, September 10-12, 1991, 108.
- Van Herwaarden, A. W., Van Duyt, D. C., Van Heusden, B. W., and Sarro, P. M., Integrated Thermopile Sensors, *Sensors and Actuators*, A21-A23, 621, 1989.
- Rose, D. M., Miniature Thermoelectric Converters, U.K. Patent No. 87 14698, 1988.
- Goldsmid, H. J., *Electronic Refrigeration*, Pion Limited, London, 1986.
- Smith, G. E. and Wolfe, R., Thermoelectric properties of bismuth antimony alloys, *J. Appl. Phys. (USA)*, 33 (3), 841, 1962.
- Debs, R. T., The prospect of Ettinghausen and Peltier cooling at low temperatures, *Br. J. Appl. Phys.*, 13 (9), 440, 1962.
- Goldsmid, H. J., Gopinathan, K., Matthews, D. N., Taylor, K. N. R., and Baird, C. A., High T_c superconductors as passive thermometers, *J. Phys. D: Appl. Phys.*, 21 (2), 344, 1988.
- Vedernikov, M. V., Kuznetsov, V. L., Duman, A. V., Melikh, B. T., and Barkov, A. T., Efficient thermoelectric cooler with a thermoelectrically passive high T_c superconducting leg, *Proc. Xth Int. Conf. Thermoelectrics*, Cardiff, Wales, September 10-12, 1991, 96.
- Sidorenko, N. A. and Massilov, A. B., Cryogenic thermoelectric coolers with passive high T_c superconducting legs, *Proc. Xth Int. Conf. Thermoelectrics*, University of Texas at Arlington, October 7-9, 1992, 289.
- Stordeur, M. and Sobotta, H., Valence band structure and thermoelectric figure-of-merit of (Bi_{1-x}Sb_x)₂Te₃ single crystals, *Proc. Int. European Conf. Thermoelectrics*, Rose, D. M., Ed., Cardiff, Wales, 1988, 209.

28. Bhandari, C. M. and Rowe, D. M., Theoretical analysis of the thermoelectric figure-of-merit, *Energy Conservation and Management*, 20, 113, 1980.
29. Bhandari, C. M. and Rowe, D. M., *Thermal Conductors in Semiconductors*, Wiley Eastern Ltd., 1988.
30. Vining, C. B., The thermoelectric figure-of-merit $ZT = 1$: fact or artifact, Proc. Xth Int. Conf. Thermoelectrics, University of Texas at Arlington, October 7-9, 1992, 223.
31. Wood, C., Materials for high temperature thermoelectric energy conversion, Proc. Int European Conf. Thermoelectrics, Row, D. M., Ed., Cardiff, Wales, 1988, 1.
32. Rowe, D. M. and Shukla, V., The effect of phonon-grain boundary scattering on the thermoelectric conversion efficiency of heavily doped fine grained hot pressed silicon germanium alloys, *J. Appl. Phys.*, 52, 7421, 1981.
33. Pisharody, R. K. and Garey, L. P., Modified silicon germanium alloys with improved performance, Proc. Xth Int. Intersector Energy Conversion Engineering Conference, San Diego, CA, August, 20-25, 1983, 1978.
34. Vining, C. B., Laskow, W., Hanson, J. O., Van der Beck, R. R., and Gorsuch, P. D., Thermoelectric properties of pressure sintered $\text{Si}_0.6\text{Ge}_{0.4}$ thermoelectric alloys, *J. Appl. Phys.*, 69, 4333, 1991.
35. Slack, G. A. and Hussain, M. A., The maximum possible conversion efficiency of silicon germanium generators, *J. Appl. Phys.*, 70 (5), 2694, 1991.
36. Rowe, D. M., Fu, L. W., and Williams, S. G. K., Comments on the thermoelectric properties of pressure sintered $\text{Si}_0.6\text{Ge}_{0.4}$ thermoelectric alloys, *J. Appl. Phys.*, 73, 4683.
37. Florial, J. P., Boisjoly, A., and Vandervande, J., Optimisation of the thermoelectric properties of hot pressed n-type SiGe materials by multiple doping and microstructure control, Proc. Xth Int. Conf. Thermoelectrics, Cardiff, Wales, September 10-12, 1991, 156.

Section A

General Principles and Theoretical Considerations

2

Thermoelectric Phenomena

Daniel D. Pollock
State University of New York
Buffalo, New York, U.S.A.

2.1 Introduction	7
2.2 Thermodynamics	9
2.3 Thermoelectric Laws	14
2.4 Absolute Thermoelectric Properties	15
Acknowledgment	17
References	17

2.1 Introduction

An electrical potential (voltage) is generated within any isolated conducting material that is subjected to a temperature gradient; this is the absolute Seebeck effect, ASE. The absolute Seebeck coefficient, ASC, is defined as the instantaneous rate of change of the ASE with respect to temperature at a given temperature: $ASC = [d(ASE)/dT]_T$. The least complicated example of the way in which this phenomenon is used is to form a thermocouple composed of two dissimilar conductors, or thermometers, by electrically joining one set of their ends. The application of a temperature difference, or gradient, between the ends of this device will produce a voltage across its unpaired terminals that is a function of the temperature distribution.¹⁻⁴

The resulting voltage is the relative Seebeck effect, RSE, Figure 1. It results only from the difference between the internal potentials, or ASEs, within the individual conductors of which it is composed. The relative Seebeck coefficient, RSC, is the instantaneous rate of change of the RSE with temperature at a given temperature: $RSC = [d(RSE)/dT]_T$. The Seebeck effect does not arise as a result of the junction of the dissimilar materials, nor is it directly affected by the Thomson or the Peltier effects; the latter two thermal effects are present only when current flows in a thermoelectric circuit and are not voltages. These responses are in contrast to that of the relative Seebeck effect, which exists as long as the temperature gradient is maintained, regardless of whether current flows or not. It turns out that the relative Seebeck potential is the driving force for the current flow that is

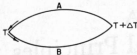


FIGURE 1 Thermodynamic circuit for the relative Seebeck coefficient. (From Pollock, D.D., *Thermoelectricity: Theory, Thermometry, Tool*, ASTM Special Technical Publication 852, American Society for Testing and Materials, Philadelphia, PA, 1985. With permission.)

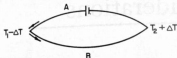


FIGURE 2 Thermodynamic circuit for the Peltier effect. (From Pollock, D.D., *Thermoelectricity: Theory, Thermometry, Tool*, ASTM Special Technical Publication 852, American Society for Testing and Materials, Philadelphia, PA, 1985. With permission.)

responsible for the Peltier and Thomson effects in thermoelectric circuits in the absence of other applied voltages.

Too frequently the RSE has been incorrectly described in the literature as being a consequence of the external contact potential, or Volta effect, between dissimilar materials. The external contact potential is not a thermoelectric effect. An external contact potential is induced when two different materials are brought sufficiently close to each other, but are not in physical contact, so that electron transfer between them results in a common Fermi energy level in each. This mechanism is independent of temperature and vanishes virtually instantaneously ($\sim 10^{-15}$ s) when the materials make physical contact. The external contact potential has no relationship whatsoever to any thermoelectric phenomena.³

The greatest application of the Seebeck effect is in thermoelectric thermometry. This results from the fact that thermoelectric circuits convert thermal energy into electrical energy. The open-circuit (null-balance) emf obtained by this means is the RSE, which can be used to measure temperature. Thermocouples composed of standardized metallic conductors are very widely used for the accurate, sensitive, and reliable measurement and/or control of temperature.

Peltier showed that heat is absorbed or liberated when a current crosses an interface between two different conductors; see Figure 2.⁴ This also occurs within nonhomogeneous conductors at concentration gradients or at phase interfaces within multiphase materials. The Peltier effect is the reversible change in the heat content at an interface between dissimilar conductors that results from the flow of current across it.

The Peltier coefficient, π_{AB} , is the change in the reversible heat content at the junction of conductors A and B when unit current flows across it in unit time, where $\pi_{AB} = \pi_A + \pi_B$ and π_A and π_B are the respective absolute Peltier coefficients of the conductors. The direction in which current flows across a junction and the values of π_A and π_B determine whether heat is liberated or absorbed. The Peltier effect is a result of the change in the entropy of the electrical charge carriers as they cross a junction. It is not an emf despite the fact that π_{AB} can be expressed in energy units involving volts. The Peltier effect, like the Seebeck effect, is unrelated to the contact potential.

For a constant current, the Peltier effect is proportional to the RSC, and at any fixed junction temperature, it is proportional to the current. These reversible effects are independent of the shape or dimensions of the junction. This is in contrast to Joule heating which is a function of dimensions,

does not require a junction, or change its sign, and is irreversible. Applications of the Peltier effect include thermoelectric devices for refrigeration and for power generation.

The Thomson effect is the reversible change of heat content within any single homogeneous conductor in a temperature gradient when an electric current passes through it. Figure 3.⁷⁻¹⁰ This may occur in any nonisothermal segment of a conductor. The Thomson coefficient is the reversible change of the heat content within a single conductor per unit temperature gradient per unit current flow. Thomson termed it the "specific heat of electricity". The Thomson effect is not a voltage, although, like the Peltier effect, it can be expressed in energy units involving volts.

The Thomson effect is a manifestation of the direction of flow of electrical carriers with respect to a temperature gradient within a conductor. These absorb energy (heat) flowing in a direction opposite to a thermal gradient, increasing their potential energy; and, when flowing in the same direction as a thermal gradient, they liberate heat, decreasing their potential energy.

2.2 Thermodynamics

The thermodynamic relationships between thermoelectric effects are important in order to understand the basic phenomena, and because the quantum mechanic treatments are based on them. The thermodynamics relates the thermoelectric effects and the quantum mechanics explains their mechanisms.¹¹

The thermodynamic analysis given here is essentially that of Thomson.^{11,12} More rigorous treatments are given by Benedict¹³ and Callen.^{13,14}

A thermoelectric circuit can be treated as very closely approximating a "reversible heat engine". The very small irreversible thermal (joule) losses can be neglected as shown in the following approximation. The current in a closed thermometric thermoelectric circuit is about 10^{-1} A. The electrical resistance of the thermocouples is small (usually minimized in order to achieve maximum sensitivity), being usually much less than $10\ \Omega$. This gives a negligible irreversible heat loss (\dot{V}^R) of considerably less than $10^{-3}\ W$.

Let two dissimilar conductors, A and B, constitute a closed circuit, see Figure 1, in which the colder junction is at temperature T and the hotter junction is at $T + \Delta T$ and both are maintained by heat reservoirs. The RSE generated by the temperature difference is E_{AB} . The RSC (the change in emf per Kelvin) is dE_{AB}/dT so the electrical energy is expressed as

$$I E_{AB} = I \frac{dE_{AB}}{dT} \Delta T \quad (1)$$

and, for unit current flowing in the thermoelectric circuit,

$$E_{AB} = \frac{dE_{AB}}{dT} \Delta T \quad (2)$$

The other energy factors in a closed thermoelectric circuit are the Peltier effects (changes in the heat contents at the junctions) and the Thomson effects (changes in the heat contents in the individual conductors). These thermal energies are expressed as:

Peltier effects (at the junctions) (3a)

$$\text{Heat absorbed at the hotter junction} = \pi_{AB}(T + \Delta T)$$

$$\text{Heat liberated at the colder junction} = -\pi_{AB}(T)$$

Thomson effects (within the conductors) (3b)

$$\text{Heat absorbed in conductor B} = \beta_B(\Delta T)$$

$$\text{Heat liberated in conductor A} = -\beta_A(\Delta T)$$

where π and β are the Peltier and Thomson coefficients, respectively.

A thermoelectric circuit approximates a reversible heat engine so the thermal and electrical energies can be equated. For unit current flow in the circuit,

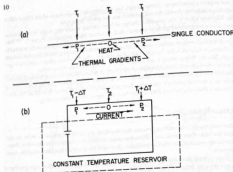


FIGURE 3. (a) Opposing thermal gradients in a single conductor in an open circuit. (b) Asymmetrical thermal gradients caused by the Thomson effect in a single conductor in a closed circuit. (From Pollock, D.D., Thermoelectricity Theory, Thermometry, Test, ASTM Special Technical Publication 852, American Society for Testing and Materials, Philadelphia, PA, 1985. With permission.)

$$\frac{dE_{AB}}{dT} \Delta T = \pi_{AB}(T + \Delta T) - \pi_{AB}(T) + (\beta_B - \beta_A)\Delta T \quad (4)$$

Equation 4 is divided through by ΔT to obtain

$$\frac{dE_{AB}}{dT} = \frac{\pi_{AB}(T + \Delta T) - \pi_{AB}(T)}{\Delta T} + (\beta_B - \beta_A) \quad (5)$$

The fraction on the right is a difference quotient. This gives, for the condition in which ΔT approaches zero, the instantaneous rate of change of the Peltier effect with respect to temperature. Thus, Equation 5 is expressed as

$$\frac{dE_{AB}}{dT} = \frac{d\pi_{AB}}{dT} + (\beta_B - \beta_A) \quad (6)$$

This is the fundamental thermodynamic theorem for closed thermoelectric circuits; it shows the energy relationship between the electrical Seebeck effect and the thermal Peltier and Thomson effects. These components of Equation 6 represent distinct thermal phenomena that are induced by the RSE that arises solely from the temperature (energy) gradient in conductors A and B. While the Peltier and Thomson effects may be expressed in energy units involving voltage, they are purely thermal in character.

It must be emphasized that Equation 6 is derived for closed circuits with no external electrical sources. The RSC, as represented by dE_{AB}/dT , is nonzero in open thermoelectric circuits, while the Peltier and Thomson heat changes are zero for this case. This arises because the current is zero, while their coefficients remain unchanged. Thus, Equation 6 does not hold for the case in which no current flows. This clearly demonstrates that the RSE should not be considered to be the physical consequence of the Peltier and Thomson effects. This may be restated as: the thermal terms in Equation 6 may not be converted to their electrical equivalents to "explain" the Seebeck effect.

The electrical Seebeck effect is the driving force for the currents that give rise to the thermal Peltier and Thomson effects in closed circuits. These thermal effects can introduce small temperature errors in thermoelectric thermometry, but the IR voltage losses can cause much larger decreases in the accuracy of such emf readings. It is for these reasons that the most accurate thermoelectric thermometry employs null-balance (open-circuit or zero-current) measurements.

The approximation that thermoelectric circuits may be treated as being thermodynamically reversible simplifies the analyses of their relationships. Thus, the net change in the entropy of the surroundings of a closed thermoelectric circuit may be approximated as being equal to zero. While this is not rigorous, it simplifies the problem and gives results that are in excellent agreement with experimental findings.¹⁴ This simplifies the analyses of the thermodynamic properties of thermoelectric circuits based on the net entropy changes of their surroundings as represented by the thermal reservoirs in the following analysis.

Two additional reservoirs are positioned at the midpoints of conductors A and B. Each of these central reservoirs is maintained at a temperature that is the average of those at the hotter and colder junctions, Figure 4. These provide a means to evaluate the average change in the entropy of the surroundings of each of the thermoelements in the circuit.

A unit quantity of electricity is made to flow through the circuit. The approximation of reversibility permits the assumption that the net change in the entropy, ΔS , of all of the reservoirs (at the junctions and along the conductors) is zero. This enables the net entropy change of the surroundings of a thermoelectric circuit to be given as

$$\Delta S = \frac{-\pi_{AB}(T + \Delta T)}{T + \Delta T} + \frac{\pi_{AB}(T)}{T} - \frac{\beta_B(\Delta T)}{T + \frac{\Delta T}{2}} + \frac{\beta_A(\Delta T)}{T + \frac{\Delta T}{2}} = 0 \quad (7)$$

The first two terms of Equation 7 are multiplied by $\Delta T/\Delta T$ to obtain

$$\Delta S = \left[\frac{-\frac{\pi_{AB}(T + \Delta T)}{T + \Delta T} + \frac{\pi_{AB}(T)}{T}}{\Delta T} \right] \Delta T - \frac{\beta_B(\Delta T)}{T + \frac{\Delta T}{2}} + \frac{\beta_A(\Delta T)}{T + \frac{\Delta T}{2}} = 0 \quad (8)$$

In the limit, as ΔT approaches zero, the difference quotient within the brackets is $-\frac{d}{dT} \left(\frac{\pi_{AB}}{T} \right)$. Its substitution into Equation 8 yields

$$\Delta S = -\frac{d}{dT} \left(\frac{\pi_{AB}}{T} \right) \Delta T - \frac{\beta_B(\Delta T)}{T + \frac{\Delta T}{2}} + \frac{\beta_A(\Delta T)}{T + \frac{\Delta T}{2}} = 0 \quad (9)$$

Using the definition of the Thomson coefficient, $\Delta T = 1K$, and since T is much greater than $1K$, $T + \Delta T/2 = T + 1/2 \approx T$. This approximation permits Equation 9 to be written more simply as

$$\frac{d}{dT} \left(\frac{\pi_{AB}}{T} \right) \approx \frac{\beta_A}{T} - \frac{\beta_B}{T} \quad (10)$$

The indicated derivative reduces Equation 10 to

$$\frac{T \frac{d\pi_{AB}}{dT} - \pi_{AB}}{T^2} \approx \frac{\beta_A}{T} - \frac{\beta_B}{T} \quad (11)$$

Equation 11 is simplified and rearranged as

$$\frac{\pi_{AB}}{T} = \frac{d\pi_{AB}}{dT} + \beta_B - \beta_A \quad (12)$$

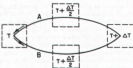


FIGURE 4 Closed thermoelectric circuit for the analysis of thermal phenomena. (From Pollock, D.D., Thermoelectricity: Theory, Thermometry, Tool, ASTM Special Technical Publication 852, American Society for Testing and Materials, Philadelphia, PA, 1985. With permission.)

Equation 12 represents the entropy change at a thermoelectric junction in a closed circuit because π_{AB} is the change in the heat content of the junction, and, divided by the absolute temperature, is (by the Nernst definition) the change in entropy of the junction for the given temperature.¹⁷

Equation 12, relating the Peltier and Thomson coefficients, is helpful as a means for the selection of materials for use in Peltier devices. Equation 12 is reexpressed for clarity as

$$-\frac{d\pi_{AB}}{dT} \equiv -\frac{\kappa_{AB}}{T} + (\beta_B - \beta_A) \quad (13)$$

If a maximum Peltier effect exists, $d\pi_{AB}/dT = 0$. This is used to obtain the optimum relationship between the two thermal effects as

$$\pi_{AB} \equiv (\beta_B - \beta_A)T \quad (14)$$

Where data are available for the Thomson coefficients, the best combinations of thermocouples may be selected by means of simple calculations.

The fundamental thermodynamic theorem (Equation 6) is used in Equation 12 to obtain

$$\frac{\pi_{AB}}{T} \equiv \frac{dE_{AB}}{dT} \quad (15)$$

Equation 15 gives the RSC of a thermocouple as a direct measure of the change in the entropy at a thermoelectric junction in closed circuits and may be rewritten as

$$\pi_{AB} \equiv \frac{dE_{AB}}{dT} T \quad (16)$$

Equation 16 is helpful in understanding the operation of Peltier devices. It shows why combinations of thermocouples with large Peltier effects must be used for power generation or for refrigeration. The thermal efficiency is low in either case.

Another important relationship between the Seebeck and Thomson effects is obtained by starting with the derivative of Equation 16:

$$\frac{d\pi_{AB}}{dT} \equiv \frac{dE_{AB}}{dT} + T \frac{d^2E_{AB}}{dT^2} \quad (17)$$

Equation 17 is reexpressed for clarity as

$$\frac{d\pi_{AB}}{dT} - \frac{dE_{AB}}{dT} \equiv T \frac{d^2E_{AB}}{dT^2} \quad (18)$$

A similar expression is obtained from Equation 6:

$$\frac{d\pi_{AB}}{dT} - \frac{dE_{AB}}{dT} \approx -(\beta_B - \beta_A) \quad (19)$$

Equations 18 and 19 are equated to obtain

$$T \frac{d^2 E_{AB}}{dT^2} \approx -(\beta_B - \beta_A) \quad (20)$$

which can be rewritten as

$$\frac{d^2 E_{AB}}{dT^2} \approx \frac{\beta_A - \beta_B}{T} \quad (21)$$

The integration of Equation 21 provides the relationship being sought in the form of

$$\frac{dE_{AB}}{dT} \approx \int_0^T \frac{\beta_A - \beta_B}{T} dT \approx \int_0^T \frac{\beta_A}{T} dT - \int_0^T \frac{\beta_B}{T} dT \quad (22)$$

Equation 22 is integrable because the quantities β/T are entropies, and based on the third law of thermodynamics, they approach zero as the temperature approaches zero.¹⁷ On this basis, the thermoelectric energy of a thermocouple in a simple closed circuit is responsible for the difference between the entropies of the components of which it is composed. The restrictions noted for Equation 6 also hold for Equation 22. The Seebeck effect may not be ascribed to the algebraic difference of Thomson effects.

The use of Equation 22 in Equation 16 leads to another important relationship between the Thomson and Peltier coefficients. For closed thermoelectric circuits,

$$\pi_{AB} = \frac{dE_{AB}}{dT} T = \left(\int_0^T \frac{\beta_A}{T} dT - \int_0^T \frac{\beta_B}{T} dT \right) T \quad (23)$$

Equation 23 may be simplified as

$$\pi_{AB} = \pi_A - \pi_B \quad (24)$$

In other words, since the integrals in Equation 22 are entropies, π_A and π_B are the entropies of the individual components forming a thermoelectric junction. Thus, the Peltier effect arises as a result of the entropy difference between the components of a junction. Heat (energy) is evolved when the carriers flow from a component with higher entropy to one with lower entropy. Heat is absorbed in the opposite case.

Equation 24 is one of the bases for the statements made earlier that the Peltier effect has no relation to contact potential.

Equation 22 permits the RSC of a thermocouple in a closed circuit to be given in terms of the entropy difference between its components. It is the thermodynamic basis for the concept that in terms of the energies involved, the RSC of a thermocouple is the algebraic sum of the ASCs of its component thermoelements. However, despite its common misinterpretation, Equation 22 does not hold for open-circuit emf measurements because, as noted in reference to Equation 6, the Thomson heat changes are zero, and the RSC is nonzero for this case.

The independence of the RSC of the Thomson effects arises solely from the fact that the potential difference (ASE) that exists in each of the thermoelements composing a thermocouple in a temperature gradient is present in open circuits. And, in a way analogous to Equation 22, the open-circuit RSC of a thermocouple is given by

$$\frac{dE_{AB}}{dT} = \alpha_A - \alpha_B \quad (25)$$

in which α_A and α_B are the ASCs of its components. Equation 25 is of fundamental importance because it permits the study and evaluation of the properties of individual thermoelements without

the need for recourse to any other thermoelements. The natures of α_A and α_B are best described by quantum mechanics, rather than thermodynamics, because of the special properties of the electrical carriers involved.¹¹

One of the least complicated ways to visualize the concept of absolute Seebeck properties is to consider a thermocouple made of a normal conductor and a superconductor. The ASCs of superconductors are zero at temperatures lower than that at which they undergo the transition to superconductivity.¹² A temperature gradient induces no potential difference (emf) within the superconductor (its ASE equals zero), but does produce one in the normal conductor. The emf generated by this thermocouple is just originating in the normal thermoelement. At present, this technique is applicable to temperatures below about 120 K.

Elemental lead (Pb) is sometimes used for thermoelectric reference purposes. This means that it is used as a reference thermocouple (with established thermoelectric properties) as one leg of a thermocouple. The ASCs of other thermoelectric materials then are calculated using Equation 25. One reason lead is used is that its ASC is comparatively small with respect to most other thermoelectric materials. So, when lead is used as a reference thermoelement, the RSC of the thermocouple largely arises as a result of the ASC of the other thermoelement. This technique is limited by the relatively low melting point of Pb, and it now is used for reference purposes at temperatures below room temperature.

Very pure platinum now is generally used as a reference thermoelement. Its high melting point, established thermoelectric properties, and stability in oxidizing atmospheres make it more useful over a broader range than lead.

Reference materials with formally standardized ASCs are yet to be established.

The thermodynamic reference temperature and that of absolute thermoelectric properties is 0 K. Equation 22. Any convenient, readily reproducible temperature can be used for practical reference purposes. The melting point of ice at one atmosphere pressure, 0°C, is most generally used in thermometry as the practical reference temperature because of its ready availability and ease of practical reproducibility.¹³

2.3 Thermoelectric Laws

The relationships discussed here were developed primarily for thermoelectric thermometry. When two thermoelements of the same homogeneous material form a thermocouple, no emf will be produced because α_A and α_B in Equation 25 are identical.

It also follows from Equation 25 that if no temperature difference exists between the ends of a homogeneous conductor, the net emf along the conductor will be zero even though temperature gradients exist between its ends. In this case any number of conductors can be connected in series and their net emf will be zero. Series of conductors can be made to form the measuring junction of a thermocouple with no effect on its calibration. This effect is included in the *Law of Intermediate Conductors* that states that the ASCs of any homogeneous conductors are zero when their ends are at the same temperature.

Another law of the same name states that the RSCs of two thermocouples composed of thermometers A-C and C-B, each of whose junctions are at the same temperatures, may be expressed as $dE_{AB}/dT = \alpha_A - \alpha_C + \alpha_C - \alpha_B = \alpha_A - \alpha_B$. Thermometers, such as Pt, that are common to both thermocouples are used in this way to pair thermoelements. In this case the contribution of the common thermometer is denoted above by α_C .

A fourth law is the *Law of Successive Temperatures*. This law is a consequence of integrating Equation 25 over successive temperature ranges, where T_0 is a reference temperature and $T_0 < T_1 < T_2 < T_3$.

$$E_{AB} = \int_{T_0}^{T_1} (\alpha_A - \alpha_B) dT + \int_{T_1}^{T_2} (\alpha_A - \alpha_B) dT + \int_{T_2}^{T_3} (\alpha_A - \alpha_B) dT \quad (26)$$

which is the same as

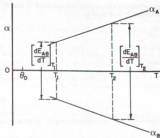


FIGURE 5 Schematic diagram of the thermoelectric properties of a thermocouple in terms of its component thermocouples. (From Pollock, D.D., Thermoelectricity: Theory, Thermometry, Tool, ASTM Special Technical Publication 852, American Society for Testing and Materials, Philadelphia, PA, 1985. With permission.)

$$E_{AB} = \int_{T_0}^{T_1} (\alpha_A - \alpha_B) dT \quad (26a)$$

In effect, the emf of a given thermocouple composed of homogeneous thermocouples can be measured or represented by the sum of its emfs over successive temperature ranges. This is very useful in the calibration of thermocouples and in the establishment of emf-temperature characteristics over wide temperature ranges. Equation 26 is also of help in understanding the influence of circuitry, including extension wires, in thermoelectric thermometry.²⁰

2.4 Absolute Thermoelectric Properties

Thermocouple properties can only be explained by the concept of absolute thermoelectric properties because, as was shown previously,

$$\frac{dE_{AB}}{dT} = \alpha_A - \alpha_B \quad (25)$$

In other words, the ASC of each component of a thermocouple must be understood in order to understand the thermoelectric properties of a thermocouple.²⁰ Two widely differing pairs of thermocouples are discussed here as a means of understanding the thermoelectric characteristics of most thermocouples.

The first case is that of two thermocouples whose ASCs have both different signs and slopes; Figure 5. The RSC of thermocouple A-B is obtained graphically from Figure 5 for any temperature by means of the algebraic sum indicated by Equation 25.

The individual ASCs of the thermocouples A and B are given for $T > T_0$, where T_0 is the Debye temperature, as

$$\alpha_A = C_1 + m_A T \quad (27a)$$

and

$$\alpha_B = C_2 + m_B T \quad (27b)$$

Here C_0 and C_1 are empirical constants and the respective slopes are m_B and m_A . The RSE of thermocouple A-B, Equation 25, is obtained as

$$\frac{dE_{AB}}{dT} = C_0 + (m_B - m_A)T \quad \text{or} \quad dE_{AB} = [C_0 + (m_B - m_A)T]dT \quad (28)$$

where another empirical constant $C_2 = C_1 - C_0$. Equation 28 represents an element of area between the curves so that the RSE generated by thermocouple A-B is the area between the curves obtained by integration over the temperature range between the reference and measuring junctions. It will be noted that the lower temperature (reference temperature) may be selected as that being most convenient. If the reference junction is selected and maintained at a given temperature, T_o , the emf of thermocouple A-B is expressed using Equation 28 as

$$E_{AB} = \int_{T_o}^T [C_0 + (m_B - m_A)T]dT \quad (29)$$

The integration of Equation 29 over the temperature range of interest gives the emf of thermocouple A-B as

$$E_{AB} = C_0(T - T_o) + 1/2 \cdot (m_B - m_A)(T^2 - T_o^2) \quad (30a)$$

or as

$$E_{AB} = E_o + C_0(T - T_o) + 1/2 \cdot (m_B - m_A)(T^2 - T_o^2) \quad (30b)$$

where E_o is a constant of integration, when Equation 26 is used, to account for the emf between δK and T_o . Equation 30b includes a term that contains the difference of squares of the temperatures. It is a nonlinear function of temperature. High degrees of thermoelectric nonlinearity were originally considered to be undesirable for use in thermometry because they required both more complex expressions than those given by Equations 30a and 30b and correspondingly more expensive measuring/controlling instrumentation. This problem is no longer of concern with contemporary equipment.

The most desirable situation is one in which the ASGs of two thermoelements A and D are parallel functions of temperature. In this ideal case, the slopes will be equal ($m_A = m_D = m$) and the ASGs are given by

$$\alpha_A = C_1 + mT \quad (27a)$$

and

$$\alpha_D = C_4 + mT \quad (31)$$

Then, $\alpha_0 - \alpha_A = C_4 - C_1 = C_3$, another constant, because the temperature-dependent terms vanish, and the RSE of couple A-D is

$$\frac{dE_{AD}}{dT} = C_4 - C_1 = C_3 \quad (32)$$

Thus, the RSE of this thermocouple is

$$E_{AD} = \int_{T_o}^T C_3 dT = C_3(T - T_o) \quad (33)$$

where T_o again is a reference temperature.

The emf of couple A-D is a linear function of the temperature difference. A relationship of this kind was considered by manufacturers of thermometric devices to be ideal when contrasted to that shown by couple A-B, Equation 30a. Components associated with thermoelectric thermometry and electrical circuits based on linear behavior are more readily made and calibrated than those based on nonlinear responses of sensing devices. This would simplify the production of more accurate and more economical temperature measuring and control devices.

This practical consideration is one of the reasons for the relatively few combinations of metals and alloys in common use as components of standard thermocouples. While no two thermocouple alloys have exactly the same slopes, pairs of thermocouples are available with relatively small differences between their slopes, Equation 27. This causes the quadratic term of Equation 30a to be relatively small compared to the linear term. None of these thermocouples have ideally linear thermoelectric characteristics. To a good first approximation such thermocouples are considered to approach a linear emf-temperature characteristic.

On the basis of the foregoing, it is seen that the temperature-dependent terms of Equations 27a and 27b are of fundamental importance in the understanding of the absolute thermoelectric properties of thermocouple elements. As noted previously, these are best described by quantum mechanics because of the nature of the electrical carriers.¹¹

Acknowledgment

I am deeply indebted to Dr. R.P. Reed, of the Sandia National Laboratories, for his helpful comments and for the terminology used in this chapter.

References

1. Seebeck, T. J., Ueber den magnetismus der galvanische kette, *Abh. K. Akad. Wiss. Berlin*, 289, 1821.
2. Seebeck, T. J., Magnetische polarisation der metalle und erze durch temperatur-differenz, *Abh. K. Akad. Wiss. Berle*, 265, 1823.
3. Seebeck, T. J., *Anz. Phys. (Leipzig)*[2], 6, 1, 1826.
4. Seebeck, T. J., Methode, Platinriegel auf ihr chemische reinheit durch thermomagnetismus zu prufen, *Schweigger's J. Phys.*, 46, 101, 1826.
5. Pollock, D. D., *Physics of Engineering Materials*, Prentice Hall, Englewood Cliffs, NJ, 1990, 330.
6. Peltier, J. C. A., Nouvelles experiences sur la calorite des courants electriques, *Ann. Chem. Phys.*, 56, 571, 1834.
7. Thomson, W., An account of Carnot's theory of the motive power of heat, *Proc. R. Soc. Edinburgh*, 16, 541, 1849.
8. Thomson, W., On a mechanical theory of thermo-electric currents, *Philos. Mag.* [5], 3, 529, 1852.
9. Thomson, W., Account of researches in thermo-electricity, *Philos. Mag.* [5], 8, 62, 1854.
10. Thomson, W., On the electrodynamic qualities of metals, *Philos. Trans. R. Soc. London*, 146, 649, 1856.
11. Pollock, D. D., *Thermoelectric Theory and Properties*, CRC Press, Boca Raton, FL, 1991, chap. 5.
12. Bridgeman, P. W., *The Thermodynamics of Electrical Phenomena in Metals*, Dover, New York, 1961, chap. 2.
13. Roemer, F., Thermoelectric Thermometry, *J. Appl. Phys.*, 11, 388, 1940.
14. Benedict, R. P., *Fundamentals of Temperature, Pressure and Flow Measurements*, 3rd ed., Wiley-Interscience, New York, 1984, chap. 7.
15. Callen, H. B., Application of Onsager's reciprocal relations to thermoelectric, thermomagnetic and galvanomagnetic effects, *Phys. Rev.*, 78, 1348, 1948.
16. Callen, H. B., Irreversible thermodynamics of thermoelectricity, *Rev. Mod. Phys.*, 26, 237, 1954.
17. Durkun, L. S. and Gurry, R. W., *Physical Chemistry of Metals*, McGraw-Hill, New York, 1953, 191.
18. Pollock, D. D., *Physical Properties of Materials for Engineers*, CRC Press, Boca Raton, FL, 1993, sect. 6.8.3.
19. Roemer, W. F. and Lorberger, S. T., *Methods of Testing Thermocouples and Thermoelectric Materials*, NBS Circular 590, National Bureau of Standards, U.S. Government Printing Office, Washington, D.C., 1958.
20. Reed, R. P., Thermoelectric thermometry: a functional model, in *Temperature, Its Measurement and Control in Science and Industry*, 5, American Institute of Physics, New York, 1982, 913.
21. Thomson, W., On an absolute thermometric scale, *Philos. Mag.* [4], 33, 313, 1848.

3

Conversion Efficiency and Figure-of-Merit

H. J. Goldsmid
University of New South Wales,
Australia

3.1 Ideal Model	19
3.2 Thermoelectric Refrigeration	19
Cooling Power • Figure-of-Merit • Coefficient-of- Performance • Multistage Refrigerators	
3.3 Thermoelectric Generation	24
3.4 Temperature-Dependent Parameters	25
References	25

3.1 Ideal Model

In order to obtain an expression for the conversion efficiency of a thermoelectric device, the rather idealized thermocouple shown in Figure 1 is considered. The thermocouple consists of a positive (p) and negative (n) branch (thermoelement) to which are attached metallic conductors A, B, and C of supposedly zero electrical resistance. The branches are of length L_p and L_n and of cross section area A_p and A_n where, in general, the ratios L_p/A_p and L_n/A_n are different from one another. In spite of suggestions to the contrary,¹ the steady-state condition is unaffected by the shape of the branches; they are shown of constant cross section area merely for convenience. An important assumption is that heat is transferred from the heat source at B to the heat sink at AC solely by conduction along the branches of the thermocouple. It should be clear that the connection of any number of such couples, electrically in series and thermally in parallel, affects the power handling capacity of the converter but not its efficiency.

The thermocouple can be used in two ways. If a voltage source is connected across A and C so that an electric current is driven through the couple, it acts as a heat pump (or, more specifically, if A is negative and C positive, a refrigerator). Heat is pumped from the source at an absolute temperature T_1 to the heat sink at temperature T_2 by means of the Peltier effect. Alternatively, if a resistive load is placed across A and C, the supply of heat at B and its removal at AC causes an electric current to flow around the circuit due to the Seebeck effect; in other words, the thermocouple acts as a generator. It can be shown that the coefficient of performance of the couple when used as a refrigerator and its efficiency when used as a generator can both be related to a parameter, known as the figure-of-merit, that incorporates certain of the material properties of the two arms.

3.2 Thermoelectric Refrigeration

Cooling Power

The theory of the thermoelectric refrigerator will be discussed first. It is important to realize that, although the Peltier and Seebeck effects require junctions between thermoelements for their manifestation, they are essentially bulk phenomena, i.e., they depend on bulk rather than surface properties of the materials. Thus, when an electric current flows through a conductor it transports heat, which reveals itself in the Peltier effect when it has to be liberated or absorbed as the current passes

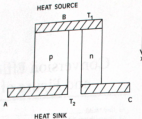


FIGURE 1. Thermocouple for heat pumping or generation.

into another conductor in which the heat transported is different. Thus, in the two branches, the heat transported from the source to the sink is

$$\left. \begin{aligned} q_p &= \alpha_p IT - \lambda_p A_p dT/dx \\ q_n &= -\alpha_n IT - \lambda_n A_n dT/dx \end{aligned} \right\} \quad (1)$$

in the two branches respectively, where α is the absolute Seebeck coefficient, I is the current, λ is the thermal conductivity, and dT/dx is the temperature gradient. From Kelvin's second law, the Peltier coefficient is given by αIT , where T is the absolute temperature. It should be noted that α_p is positive and α_n is negative so that, in both cases, the Peltier heat flow off IT is opposed by the heat conduction $\lambda dT/dx$.

The rate of heat generation per unit length within each branch, due to the Joule effect, is P_0/A , where P is the electrical resistivity, which is the reciprocal of the electrical conductivity σ . This heat generation implies that the temperature gradient is nonuniform, where

$$\left. \begin{aligned} -\lambda_p A_p \frac{dT}{dx^2} &= \frac{P_0}{A_p} \\ -\lambda_n A_n \frac{dT}{dx^2} &= \frac{P_0}{A_n} \end{aligned} \right\} \quad (2)$$

For the present purposes it is assumed that the Seebeck coefficient is independent of temperature, which means that the Thomson effect is absent. This assumption can be reconsidered later.

Setting the boundary condition that $T = T_1$ at $x = 0$ (i.e., at the heat source) and also setting $T = T_2$ at $x = l_p$ or l_n (i.e., at the heat sink), Equation 2 can be solved to find

$$\left. \begin{aligned} \lambda_p A_p \frac{dT}{dx} &= -\frac{P_0}{A_p} \left(x - \frac{l_p}{2} \right) + \frac{\lambda_p A_p (T_2 - T_1)}{l_p} \\ \lambda_n A_n \frac{dT}{dx} &= -\frac{P_0}{A_n} \left(x - \frac{l_n}{2} \right) + \frac{\lambda_n A_n (T_2 - T_1)}{l_n} \end{aligned} \right\} \quad (3)$$

Equations 1 and 3 can be combined to obtain the rate of heat flow at $x = 0$,

$$\left. \begin{aligned} q_p(x=0) &= \alpha_p IT_1 - \frac{\lambda_p A_p (T_2 - T_1)}{l_p} - \frac{P_0}{2 A_p} l_p \\ q_n(x=0) &= -\alpha_n IT_1 - \frac{\lambda_n A_n (T_2 - T_1)}{l_n} - \frac{P_0}{2 A_n} l_n \end{aligned} \right\} \quad (4)$$

If, then, q_p and q_n are added at $x = 0$, the cooling power q_C at the heat source is obtained,

$$q_C = (\alpha_p - \alpha_n)IT_1 - K(T_2 - T_1) - PR/2 \quad (5)$$

where the thermal conductance of the two branches in parallel is

$$K = \frac{\lambda_p A_p}{L_p} + \frac{\lambda_n A_n}{L_n} \quad (6)$$

and the electrical resistance of the two branches in series is

$$R = \frac{L_p \rho_p}{A_p} + \frac{L_n \rho_n}{A_n} \quad (7)$$

Equation 5 reveals the interesting result (often assumed without proof) that half the Joule heating ($PR/2$) arrives at the heat source while, presumably, the other half turns up at the heat sink.

Figure-of-Merit

When Equation 5 is inspected, it is seen that the Peltier cooling term $(\alpha_p - \alpha_n)IT_1$ varies linearly with the electric current I , whereas, of course, the Joule heating term $PR/2$ varies as the square of the current. This means that there must be a particular current I_q at which the cooling power reaches its maximum value. This current is easily found by setting $dq_C/dI = 0$ which occurs when

$$I_q = \frac{(\alpha_p - \alpha_n)T_1}{R} \quad (8)$$

and the maximum cooling power is then

$$(q_C)_{\max} = \frac{(\alpha_p - \alpha_n)^2 T_1^2}{2 R} - K(T_2 - T_1) \quad (9)$$

This equation reveals that a positive cooling effect cannot be achieved if the temperature difference between the junctions is too great. In fact, there is a maximum temperature difference $(T_2 - T_1)_{\max}$ which is found by setting $(q_C)_{\max} = 0$. Clearly,

$$(T_2 - T_1)_{\max} = \frac{(\alpha_p - \alpha_n)^2 T_1^2}{2 K R} \quad (10)$$

The figure-of-merit of the thermocouple is defined as

$$Z = \frac{(\alpha_p - \alpha_n)^2}{K R} \quad (11)$$

so Equation 10 can be rewritten as

$$(T_2 - T_1)_{\max} = \frac{1}{2} Z T_1^2 \quad (12)$$

It will be shown later that the same figure-of-merit applies for thermoelectric generation. However, at this point, some of the implications of Equation 12 should be considered. Also, the usual situation should be discussed where the required temperature difference $(T_2 - T_1)$ is less than the maximum that can be achieved.

Thermoelectric refrigeration is unlikely to be practical unless the maximum temperature difference is a significant fraction of the absolute temperature. For example, this method of cooling would be dismissed out of hand if it were not able to yield a source temperature $T_1 = 273$ K (i.e., 0°C) with a sink temperature of, say, $T_2 = 303$ K (i.e., 30°C). If these values are substituted into Equation 12 it is found that they correspond to a value of Z equal to 0.8×10^{-3} K $^{-1}$. This was,

in fact, the order of magnitude of the figure-of-merit for the thermocouples available in the early 1950's when development work started on new thermoelectric materials based on semiconductors.^{2,3} This work eventually led to thermocouples having a figure-of-merit of the order of $3 \times 10^{-3} \text{ K}^{-1}$ with a corresponding maximum temperature depression of some 80 K.⁴ Sometimes use can be made of the dimensionless figure-of-merit ZT instead of Z and it becomes clear that, in seeking new thermoelectric materials, one should be looking for values of ZT of the order of unity or greater.

It will be apparent that the figure-of-merit Z , as defined by Equation 12, is a characteristic not of a pair of materials but, rather, of a particular couple, since it includes terms that involve the relative dimensions of the thermocouples. For a given pair of materials, the highest value of Z is reached when the product RK is minimized. Of course, R rises and K falls as the ratio of length to cross section area increases and, indeed, a thermocouple can be designed for a given cooling power and electric current by altering the ratio in both arms. What is important, however, is to maintain a preferred relationship between L/λ in one arm and the other. It is, in fact, a trivial exercise to show that RK is minimized when

$$\frac{l_p A_p}{l_n A_n} = \left(\frac{\rho_p \lambda_n}{\rho_n \lambda_p} \right)^{1/2} \quad (13)$$

When this equation is satisfied it is indeed possible to talk about the figure-of-merit of a pair of materials, giving it the value

$$Z = \frac{(\alpha_p - \alpha_n)^2}{[(\lambda_p \rho_p)^{1/2} + (\lambda_n \rho_n)^{1/2}]^2} \quad (14)$$

This figure-of-merit embodies the properties that common sense leads us to expect to be relevant. The Seebeck (and Peltier) coefficients are required to be large and of opposite signs in the two materials. In addition the thermal conductivity and the electrical resistivity should be low. In other words, the reversible thermoelectric effects should dominate over the irreversible effects of heat conduction and Joule heating.

Actually, Equation 14 is rather cumbersome when attempting to find a good thermoelectric material, be it *p*-type or *n*-type, since it involves the properties of both thermocouples. It is for this reason that the figure-of-merit of a single material is encountered, defined as

$$z_{p,n} = \frac{\alpha_{p,n}^2}{\rho_{p,n} \lambda_{p,n}} \quad (15)$$

Only in special cases can this figure-of-merit z be accurately related to the true figure-of-merit Z . One such case is when the *p*-type and *n*-type materials are exactly equivalent to one another apart from the sign of the Seebeck coefficient. In other words $\alpha_p = -\alpha_n$ and $\lambda_p \rho_p = \lambda_n \rho_n$. Then $Z = z_p = z_n$. It is fortunate that this situation holds, at least approximately, for the materials that are used in thermoelectric refrigeration at ordinary temperatures.

Another case of some practical importance occurs when λp for one branch is negligibly small compared with that for the other branch. This is true, for example, if one of the branches is a superconductor.⁵ If an *n*-type thermocouple, say, is combined with a superconductor to form a couple, the denominator on the right-hand side of Equation 14 becomes equal to $\lambda_n \rho_n$. Furthermore, the absolute Seebeck coefficient of any superconductor is effectively zero so the numerator becomes α_n^2 and then $Z = z_n$.

It will be realized that the common practice of equating the figure-of-merit of a couple with the average of the values of z for the two branches can lead to substantial errors but the single-material figure-of-merit is widely used in the literature and there is no doubt that it is of conceptual value. There does not seem to be any better quantity to employ when dealing with just one material.

Coefficient-of-Performance

Turning now to the optimization of the current through a refrigerating couple when $(T_2 - T_1)$ is less than its maximum value, the performance of any refrigerator is usually assessed in terms of a quantity known as the coefficient of performance ϕ , defined as the ratio q_c/W , where W is the rate at which electrical energy is supplied. Looking at the branches separately,

$$\left. \begin{aligned} W_p &= \alpha_p I (T_2 - T_1) + \frac{\beta \rho_p L_p}{A_p} \\ W_n &= -\alpha_n I (T_2 - T_1) + \frac{\beta \rho_n L_n}{A_n} \end{aligned} \right\} \quad (16)$$

It will be seen that electrical power is used to overcome the Seebeck effect as well as the Joule effect. The total power is

$$W = (\alpha_p - \alpha_n) I (T_2 - T_1) + PR \quad (17)$$

The coefficient-of-performance is

$$\phi = \frac{q_c}{W} = \frac{(\alpha_p - \alpha_n) I (T_2 - T_1) - \frac{1}{2} PR - K (T_2 - T_1)}{(\alpha_p - \alpha_n) I (T_2 - T_1) + PR} \quad (18)$$

It is found that the optimum current, i.e., the one that yields the maximum coefficient-of-performance, by setting $d\phi/dI$ equal to zero. This gives a current

$$I_q = \frac{(\alpha_p - \alpha_n)(T_2 - T_1)}{R[(1 + Z T_M)^{1/2} - 1]} \quad (19)$$

where T_M , equal to $(T_1 + T_2)/2$, is the mean temperature. The corresponding coefficient-of-performance is

$$\phi_{\max} = \frac{T_2[(1 + Z T_M)^{1/2} - T_2/T_1]}{(T_2 - T_1)[(1 + Z T_M)^{1/2} + 1]} \quad (20)$$

Multistage Refrigerators

It has been seen that there is a limit to the temperature depression that can be achieved using a single-stage refrigerator. However, in principle (but not in practice) any required temperature depression can be achieved (provided that T_1 is above the absolute zero) by using thermoelectric refrigerators in cascade. Multistage units are also of some use in improving the coefficient-of-performance when the temperature depression is close to the limit for a single stage.

The optimum design of a multistage thermoelectric refrigerator is no simple matter since the effective figure-of-merit for one stage is bound to be different from that for some other stage at a different mean temperature. However, something of the problem can be appreciated by discussing the general case.

Suppose that there are N stages, the N th stage being that which operates at the lowest temperature. Then the n th stage ($n < N$) must have a cooling power that is the sum of that at the source and the electrical power used at N , $(N-1)$, ..., and $(n+1)$ stages. The coefficient-of-performance (COP) of the n th stage is designated ϕ_n and the cooling power at the N th stage as q_N . The rate of working for the n th stage is $q_N(1 + 1/\phi_N)(1 + 1/\phi_{N-1}) \dots (1 + 1/\phi_{n+1})$ and heat is delivered to the sink at the rate $q_N(1 + 1/\phi_N)(1 + 1/\phi_{N-1}) \dots (1 + 1/\phi_1)$. The overall COP is $\phi = [(1 + 1/\phi_N)(1 + 1/\phi_{N-1}) \dots (1 + 1/\phi_1) - 1]/q_N$.

In order to get some idea of the likely value of the overall COP it can be assumed that each of the stages operates at some COP ϕ' . Then $\phi = [(1 + 1/\phi')^N - 1]/q_N$. By using this relation it can easily be shown that the overall COP is going to be very low whenever the required temperature

difference is significantly greater than the maximum for a single stage. Nevertheless, multistage refrigerators using as many as six or more stages have been produced for special applications.

A common feature of all multistage refrigerators is their pyramidal shape. The N th stage consists of no more than one or two thermocouples. Then, if the same current is used throughout, subsequent stages use rapidly increasing numbers of couples so as to pump the ever-increasing amount of heat that has to be passed on.

3.3 Thermoelectric Generation

Suppose that a load of resistance R_L is connected across the thermocouple in Figure 1 at A and C. It will also be supposed that the source supplies heat at the rate q so as to maintain a temperature difference $(T_1 - T_2)$ between the junctions. The emf produced by the generator is $(\alpha_p - \alpha_n)(T_1 - T_2)$ and this yields useful power across the load given by

$$W = \left[\frac{(\alpha_p - \alpha_n)(T_1 - T_2)}{(R_L + R)} \right]^2 R_L \quad (21)$$

Next, consider the rate at which heat is supplied by the source. Most of this heat is conducted to the sink through the thermocouple brackets but it should not be forgotten that some is used to balance the Peltier effect associated with the flow of current. Also, just as for the case of thermoelectric refrigeration, half of the Joule heating in the arms finds its way to the source. If all these terms are included

$$q = K(T_1 - T_2) + (\alpha_p - \alpha_n)IT_1 - I^2R/2 \quad (22)$$

where the current I is equal to $(\alpha_p - \alpha_n)(T_1 - T_2)/(R_L + R)$. The efficiency η is equal to W/q and its value depends to some extent on the way that the load is matched to the resistance of the generator. The condition for maximum power transfer is obtained if R_L and R are made equal to one another. However, if this condition is satisfied, the efficiency can never exceed 50% of the ideal thermodynamic value $(T_1 - T_2)/T_1$. Therefore, it is assumed that the load resistance is chosen so as to yield maximum efficiency. If the ratio R_L/R , denoted by m , is required that $d\eta/dm = 0$. As shown by Lord,² the optimum value of m , identified as M , is given by

$$M = (1 + ZT_M)^{1/2} \quad (23)$$

Substituting this value into Equation 22, the efficiency is given by

$$\eta = \frac{(T_1 - T_2)}{T_1} \cdot \frac{(M - 1)}{(M + T_2/T_1)} \quad (24)$$

It will be seen that the ideal thermodynamic efficiency is degraded by the factor $(M - 1)/(M + T_2/T_1)$. The efficiency rises as M becomes greater. Since M depends only on the source and sink temperatures and on Z , it can be concluded that the same figure-of-merit holds for generation and refrigeration.

Consider the limiting cases of $ZT_M \ll 1$ and $ZT_M \gg 1$. When $ZT_M \ll 1$, $\eta \rightarrow [(T_1 - T_2)/T_1] |ZT_M|^{1/2} |(1 + ZT_M)|$ so that the ideal efficiency is multiplied by a factor that is very much less than unity. On the other hand, when $ZT_M \gg 1$, $\eta \rightarrow (T_1 - T_2)/T_1$, which is the ideal thermodynamic efficiency. It so happens that currently available materials yield ZT_M of the order of unity at most temperatures of interest. If $ZT_M = 1$, $M = 1.4142 \cdot (M - 1)/(M + T_2/T_1)$, of course, depends on T_2/T_1 as well as on M . Typically, for a generator using a small temperature difference (i.e., one that works off low-grade heat) T_2/T_1 is close to unity and $(M - 1)/(M + T_2/T_1)$ would be about 0.17. As T_2/T_1 rises, this factor increases somewhat, reaching 0.21 when $T_2 = 2T_1$ and about 0.29 when $T_2 \gg T_1$. It is seen, then, that it is at present possible to obtain something like one quarter of the ideal thermodynamic efficiency using thermoelectric generation.

3.4 Temperature-Dependent Parameters

It has been assumed that α , p , and k are all temperature independent. In practice, of course, this is never the case and a numerical computation must normally be made to find ϕ or η using parameters measured over the temperature range in question. Nevertheless, a reasonable estimation of the performance may be made using averaged parameters. The use of averages for p and k seems to present little difficulty, since the irreversible effects that they characterize are taking place throughout the elements. Ioffe,² in fact, has proposed the averaging of the product $p k$ rather than the separate parameters over the range of temperature that is applicable.

The Seebeck coefficient presents a little more difficulty. Consider the case of the thermoelectric refrigerator. Then there will be additional heating or cooling depending on the sign of the Thomson coefficient $\gamma = T_d \alpha dT$. It has been shown³ that if the average value of α over the required temperature range is used, rather than the value at the cold junction, this takes care of the Thomson effect for most practical purposes. Thus, it is reasonable to use a figure-of-merit given by

$$Z = \frac{\langle \alpha_p - \alpha_n \rangle^2}{\langle \langle p_p k_p \rangle^{1/2} + \langle p_n k_n \rangle^{1/2} \rangle^2} \quad (25)$$

where the angular brackets indicate temperature-averaged quantities. This approach is more likely to give a better approximation for thermoelectric refrigeration, where the temperature differences are generally a small fraction of the absolute temperature, than for thermoelectric generation, where the temperature differences can be much larger.

References

1. Landeker, K., *Proceedings, First International Conference on Thermoelectric Energy Conversion*, Arlington, Texas, IEEE, New York, 1976, 190.
2. Ioffe, A. F., *Semiconductor Thermocouples and Thermoelectric Cooling*, Infosearch, London, 1957.
3. Goldsmid, H. J. and Douglas, R. W., *Br. J. Appl. Phys.*, 5, 1954, 386.
4. Rosi, F. D., Abela, B., and Jensen, R. Y., *J. Phys. Chem. Solids*, 10, 1959, 191.
5. Goldsmid, H. J., Gopinathan, K. K., Matthews, D. N., Taylor, K. N. R., and Baird, C. A., *J. Phys. D Appl. Phys.*, 21, 1988, 344.
6. Goldsmid, H. J., *Electronic Refrigeration*, Pion, London, 1986.

4

Thermoelectric Transport Theory

C. M. Bhandari
*University of Allahabad
India*

4.1 Introduction	27
4.2 Transport Processes in Semiconductors	28
Transport Coefficients • Electron Distribution and Boltzmann Equation • Electron Scattering Mechanisms	
4.3 The Electronic Transport	29
Single Spherical Band Model • Two-Band Conduction • Multivalley Effects • Material Parameter • Intervalley Scattering	
4.4 Non-Parabolicity of the Energy Bands	33
Energy Dependence of the Effective Mass • Effect on the Transport Coefficients	
4.5 Thermal Transport	35
4.6 Photon Drag	35
4.7 In a Magnetic Field	37
4.8 Low-Dimensional Systems	37
Quantum Size Effects in Two-Dimensional Systems • Quasi-One-Dimensional Systems	
References	49

4.1 Introduction

To understand the behavior of a thermoelectric semiconductor¹⁻¹² in all its details it is desirable to have a clear understanding of the kinds of problems one may encounter. It is not possible to give a comprehensive account of the vast spectrum of semiconductor transport phenomena in the span of one chapter. Understandably, the emphasis will be on those aspects that have a relevance in thermoelectric applications. A cursory glance at the best known thermoelectric materials in various temperature ranges of operation indicates that one often has to deal with a multivalley semiconductor with or without intervalley scattering of carriers.¹³⁻¹⁸ The carriers may be scattered primarily by acoustic and optic phonons, neutral and ionized impurities, and to a lesser extent by grain boundaries.

Thermoelectric materials are usually heavily doped, and quite often narrow-band-gap materials. Both these situations make it imperative that, in a rigorous theoretical analysis, the effects of non-parabolicity of the energy bands are taken into consideration. At the upper end of the temperature range of operation of a thermoelectric device, minority-carrier effects make their presence felt, and their influence on various transport coefficients should not be overlooked. A number of material properties influence its thermoelectric behavior; on the other hand thermoelectric investigations yield valuable information about the same. In several situations even simple considerations may lead to meaningful results. Consequently, it is desirable to start with a simple representation of these and then gradually progress to more sophisticated and realistic models.

4.2 Transport Processes in Semiconductors

Transport Coefficients

The theory of thermoelectric transport is essentially the domain of transport in semiconductors with the behavior of metals of minor interest. Semiconductors display almost all the essential features and complications of transport phenomena in solids. The relevant transport processes involve a flow of charge or energy or both. These "flows" arise due to external causes such as an electric field and temperature gradient which are referred to as "forces". In general, any force may give rise to any flow and the relationships between various "forces" and "flows" define the various transport coefficients that are characteristic of electrons (and holes) and phonons in the material.^{1,19,20} Assuming that the electron and phonon systems depart only slightly from their equilibrium distributions a linear relationship can be obtained between "forces" and "flows". The choice of the "forces" depends upon certain considerations regarding the flow of electron and energy.

Consider a solid in contact with two reservoirs, one of energy, and the other of electrons. In the steady state a steady flow is maintained through the solid as are the differences in electrochemical potential (μ) and temperature (T) between the two points.

A good choice of the forces are $\text{grad}(\mu/T)$ and $\text{grad}(1/T)$. The components of the flows of electrons (\vec{j}) and of energy (w) are given by

$$\begin{aligned}-j_i &= \sum_{k=1}^3 L_k^{(1)} \frac{\partial}{\partial x_k} \left(\frac{\mu}{T} \right) + \sum_{k=1}^3 L_k^{(2)} \frac{\partial}{\partial x_k} \left(\frac{1}{T} \right) \\ w_i &= \sum_{k=1}^3 L_k^{(1)} \frac{\partial}{\partial x_k} \left(\frac{\mu}{T} \right) + \sum_{k=1}^3 L_k^{(2)} \frac{\partial}{\partial x_k} \left(\frac{1}{T} \right)\end{aligned}\quad (1)$$

The total energy flow can be written as a sum of W_e and W_p where e and p refer to the electron and phonon systems, respectively. In that case $L^{(1)} = L_e^{(1)} + L_p^{(1)}$ and the set of coefficients L_{ik} provide a complete description of the transport properties of the solid. The number of independent coefficients is reduced by taking the crystal symmetry into account.

The electric current density ($\vec{j}_e = -e\vec{i}$) and thermal current density (\vec{w}) can be expressed¹⁹ in terms of $\text{grad}(\mu)$ and $\text{grad}(T)$

$$\begin{aligned}\vec{i} &= \frac{1}{e} \sigma \cdot \text{grad}\mu - \sigma \cdot \alpha \cdot \text{grad}T \\ \vec{w} &= \left(\pi - \frac{\mu}{e} \right) \vec{i} - \lambda \cdot \text{grad}T\end{aligned}\quad (2)$$

σ , α , π , and λ are, in general, second-order tensors which are related to the coefficient $L^{(1)}$ defined earlier. The advantage of writing the electric and thermal current densities as in Equation 2 is obvious: these parameters are easily obtainable in practice.

Electron Distribution and Boltzmann Equation

Statistical methods are employed when dealing with equations involving a large number of particles. A probability distribution function of $f(\vec{k}, t, z)$ is introduced which describes the occupancy of allowed energy states. The most probable number of electrons in a volume element $d\vec{k}$ of the k -space at time t is given by $(2\pi\hbar)^{-3} f(\vec{k}, t, z) d\vec{k}$. The function f around a point may change due to a number of mechanisms: external fields, diffusion, and collision processes. The total rate of change of f is given by

$$\frac{df}{dt} = \left(\frac{\delta f}{\delta t} \right)_{\text{field}} + \left(\frac{\delta f}{\delta e} \right)_{\text{aff}} + \left(\frac{\delta f}{\delta \epsilon} \right)_{\text{coll}} \quad (3)$$

In the steady state $(df/dt) = 0$. Substituting for the field and diffusion terms

$$-\left(\frac{\delta f}{\delta t}\right)_{\text{coll}} = +\vec{v}_k \cdot \vec{\nabla}_r f + \frac{1}{h} \vec{F} \cdot \vec{\nabla}_d f \quad (4)$$

Here \vec{F} refers to an external force.

The basic problem is to solve this equation for $f(k)$. There are, in general, two methods to solve the Boltzmann equation. The variational method,¹³ although more rigorous, is unsuitable for routine use due to its complicated procedure. On the other hand the relaxation time approach is widely used and is particularly useful in data analysis. It is possible to obtain a solution of the Boltzmann equation if one assumes the existence of a relaxation time $\tau(k)$ defined by

$$\left(\frac{\delta f}{\delta t}\right)_{\text{coll}} = -\{f(\vec{k}, \vec{r}) - f_0(\vec{k})\}\tau(\vec{k}) \quad (5)$$

Electron Scattering Mechanisms

The next step is to obtain suitable expressions for the relaxation time for various electron (or hole) scattering processes. Among the important mechanisms that scatter electrons are phonons. In general, acoustic phonon scattering is invariably present, whereas in materials with two or more atoms per unit cell optical phonons also take part in the scattering. An electron in the state described by the electron wavevector \vec{k} is scattered to a state described by \vec{k}' as a result of an interaction with a phonon of wavevector \vec{q} . The problem is reduced to obtaining the matrix element of the interaction energy between initial and final states and then to calculate the transition probability. To simplify matters one usually considers the "adiabatic approximation", in which electron wavefunctions are assumed to keep pace with the ionic motion. The energy conservation condition has to be satisfied. The momentum of the electron-phonon system may be conserved (Normal or N-process) or it may change by a reciprocal lattice vector (Umklapp or U-process). The scattering terms require a knowledge of the phonon distribution which, in turn, requires knowledge of the electron distribution. The problem is simplified if the phonon distribution is replaced by its equilibrium value. The assumption implies that the electron and the phonon systems produce entropy independently of each other. This amounts to neglecting the phonon-drag effects which are a direct consequence of the coupling of the entropy production in the two systems via the electron-phonon interaction.^{13,34,35} The scattering by vibrational modes is contributed to both by acoustic and optical phonons, although the latter are significant at higher temperatures and in polar semiconductors.

4.3 The Electronic Transport

Single Spherical Band Model

In several cases it is possible to express the carrier relaxation time in terms of carrier energy E

$$\tau(E) = aE^b \quad (6)$$

s is referred to as the scattering parameter and takes different values for various scattering mechanisms. The proportionality constant "a" may, among other things, be a function of temperature.

The carrier mobility can be written as

$$\mu = (e/m_e^*) <\tau> \quad (7)$$

where m_e^* is the conductivity (inertial) effective mass, and $<\tau>$ is the average of $\tau(E)$ over all energies.

$$<\tau> = \frac{\int_0^\infty \tau(E) E^{3/2} \left(\frac{\delta f}{\delta E}\right) dE}{\int_0^\infty E^{3/2} \left(\frac{\delta f}{\delta E}\right) dE} \quad (8)$$

where $f_0 = [1 + \exp(\eta - \Theta)]^{-1}$.

η and ξ are the reduced carrier energy (E/kT) and reduced Fermi energy (E_F/kT), respectively. With the help of these equations the carrier mobility is obtained as¹⁸

$$\mu = \frac{2}{3} d(kT)^2 (e/m_e^*) F_{1/17}(\xi)/F_{1/2}(\xi) \quad (9)$$

$F(\xi)$ are Fermi integrals defined by

$$F(\xi) = \int_0^\infty \frac{x^3 dx}{[1 + \exp(x - \xi)]} \quad (10)$$

The Fermi energy depends upon carrier concentration and effective mass through the relation

$$\eta = \frac{4}{\sqrt{\pi}} (2\pi m^* kT/h^2)^{1/2} F_{1/2}(\xi) \quad (11)$$

With mobility and carrier concentrations known in terms of the Fermi energy, one can obtain the electrical conductivity. The dimensionless electrical conductivity is given by²¹

$$\sigma' = \left(\frac{k}{e} \right)^2 \frac{T}{k_L} \sigma = \beta F_{1+1/2}(\xi)/(s + 1/2)! \quad (12)$$

where

$$\beta = 2(2\pi k)^{1/2} k^2 A'/eh^3 \quad (13)$$

and

$$A' = T^{5/2} m^{-1/2} \mu/k_L \quad (14)$$

Here k_L refers to the lattice thermal conductivity.

β and A' are usually referred to as material parameters. Increased performance requires a large mobility to lattice thermal conductivity ratio and a higher value for the effective mass. The thermoelectric figure-of-merit is usually defined by $z = \alpha^2 \sigma / \lambda$ where α , σ , and λ refer to the Seebeck coefficient and electrical and thermal conductivity of the thermoelement material. A high value of the material parameter A' would indicate a high figure-of-merit.

Two-Band Conduction

A serious shortcoming of the single band conduction model is that the Seebeck coefficient tends to become very large as the Fermi level diverges from the band edge. This difficulty can be avoided by considering a second band or by making the assumption that, instead of diverging indefinitely from the band edge with a decrease in carrier concentration, the Fermi level approaches its intrinsic value.^{2,21} In the non-degenerate limit the inclusion of the second band is essential. A simple two-band model^{2,21} can be considered with both the bands having parabolic energy-wavevector relationships. There will be a contribution to the electric current density from both the bands. If the electrical conductivity contributions from the two bands are represented by σ_a and σ_b , then the total electrical conductivity is given by $\sigma = \sigma_a \sigma_b / (\sigma_a + \sigma_b)$. However, the total Seebeck coefficient is not a simple sum of the individual contributions from the two bands; rather, it is given by

$$\alpha = (\alpha_a \sigma_a + \alpha_b \sigma_b) / (\sigma_a + \sigma_b) \quad (15)$$

The electronic thermal transport can also be considered with the heat flux densities from the two bands given by¹

$$\vec{w}_e = \alpha_e T \vec{i}_e - \lambda_e \frac{\vec{\delta}T}{dx} \quad (16)$$

$$\vec{w}_h = \alpha_h T \vec{i}_h - \lambda_h \frac{\vec{\delta}T}{dx} \quad (17)$$

The contributions from the Peltier effect have been expressed in terms of partial Seebeck coefficients. To satisfy the condition of zero current (for defining thermal conductivity) i_v and i_h must be equal and opposite. This gives

$$i_v = -i_h = \frac{\sigma_v \sigma_h}{\sigma_v + \sigma_h} (\alpha_h - \alpha_v) \frac{\partial T}{\partial x} \quad (18)$$

With the help of Equations 16 and 17 one obtains

$$\lambda = \lambda_e + \lambda_h + \frac{\sigma_v \sigma_h}{\sigma_v + \sigma_h} (\alpha_h - \alpha_v)^2 T \quad (19)$$

Here λ is the electronic contribution to the thermal conductivity (usually referred to as λ_e). The total electronic contribution is not simply the sum of the conductivities of the two bands. The third term arises from the fact that a heat flow can take place without a charge flow. Electron-hole pairs are created at the hot end by the absorption of energy from the source. These pairs move down the temperature gradient and recombine at the cold end, releasing the energy of recombination. This process is sometimes referred to as bipolar thermodiffusion.²³ In narrow band gap semiconductors the inclusion of the other band in theoretical formulations significantly affects the various transport properties.

Multivalley Effects

In several semiconductors the transport properties cannot be adequately described in terms of a single spherical band model. The conduction and valence band structures possess several equivalent extrema. In silicon the conduction band has six minima along the [100] direction at points close to the zone boundary. The equal energy surfaces near the minima are ellipsoids of revolution with energy near the band edges given by^{15,20}

$$E(\vec{k}) = \frac{\hbar^2}{2} \left[\frac{k_1^2}{m_1} + \frac{k_2^2}{m_2} + \frac{k_3^2}{m_3} \right] \quad (20)$$

suffixes 1, 2, and 3 refer to the components along the principal directions of the equal energy ellipsoids. For an electron in the conduction band a density-of-states effective mass is defined (for a single valley) as

$$m_e^* = (m_1 m_2 m_3)^{1/3} \quad (21)$$

The conductivity (or inertial) effective mass is given by

$$m_s^{n-1} = \frac{1}{3} (m_1^{-1} + m_2^{-1} + m_3^{-1}) \quad (22)$$

The total density-of-states effective mass is given by

$$m_{d,i}^* = N_v^{1/3} (m_1 m_2 m_3)^{1/3} \quad (23)$$

N_v being the number of equivalent valleys in the band under consideration.

Material Parameter

The material parameter (Equation 14) determines the thermoelectric "worth" of a material. A large value for Λ' corresponds to a good thermoelectric performance. Let A'_v and A_v represent the material parameter² corresponding to a single spherical valley and that corresponding to an ellipsoidal energy surface. One can then write³

$$\frac{A'_v / A_v}{A'_v / A_v} = (m_2 m_3 / m_1 m^*)^{1/2} \frac{<\tau_v> / \lambda_v}{<\tau_s> / \lambda_s} \quad (24)$$

Here λ_1 and m_1 are the components of the thermal conductivity and effective mass tensors along the principal axis. If it is assumed that the same type of scattering is predominant in both the cases then the energy terms in the relaxation time averages cancel out. The constants appearing in the two relaxation rates can also be assumed to be the same. Further assuming that the density-of-states effective masses are the same in the two cases, one gets¹

$$A'_m/A'_1 = (m_2 m_3/m_1^2)^{1/3} (\lambda_2/\lambda_1) \quad (25)$$

Next consider N_v equivalent ellipsoidal energy surfaces of the type described. Defining the corresponding material parameter as A'_m one can write

$$A'_m/A'_1 = \frac{\lambda_2}{\lambda_m} \frac{N_v}{3} (m_1/m_2 m_3)^{1/3} [m_1^{-1} + m_2^{-1} + m_3^{-1}] \quad (26)$$

If it is assumed that the density-of-states effective mass corresponding to a single valley is the same as that for the single ellipsoidal valley and is given by Equation 23, the two transverse components can be taken to be equal, i.e., $m_2 = m_3$ and $m_1 = \gamma m_2$ and Equation 26 can be expressed as

$$A'_m/A'_1 = \frac{\lambda_2}{\lambda_m} N_v (1 + 2\gamma)/3\gamma^{2/3} \quad (27)$$

Implicit in this derivation is the assumption that the scattering of the charge carriers between different valleys can be ignored. It is concluded from these arguments that a large number of equivalent valleys tend to increase the material parameter and hence improve the thermoelectric performance. One may look at it from a different angle. The parameter Λ' is proportional to $\mu^{-2/3}$, and for N_v valleys $\mu' = N_v^{2/3} (m_1 m_2 m_3)^{1/3}$. For the case of acoustic photon scattering of the carriers one obtains

$$\mu^{-2/3} \propto m_v^{2/3} (m_1 m_2 m_3)^{1/3} \quad (28)$$

This gives

$$A'_m \propto N_v/m_v^2 \quad (29)$$

A number of equivalent extrema along with a small conductivity effective mass appears to favor the thermoelectric performance. For polar optical mode scattering similar conclusions are obtained.

Intervalley Scattering

The apparent favorable effect on the thermoelectric performance of a number of valleys in the conduction or valence bands may be offset by the presence of additional scattering of carriers between these valleys.^{11,17,18} Both high-energy acoustic and optical phonons take part in the intervalley scattering. The conservation of momentum requires that only short-wavelength phonons near the band-edge participate in the scattering. These phonons have frequencies which are almost independent of the wavevector. Which of the modes interact with the carriers depends upon the symmetries of the initial and final states. For example, in silicon there are two kinds of situations for intervalley scattering: those between opposite valleys (such as <100> to <100>), denoted as a g-process, or those between non-opposite valleys (such as <100> to <010>), referred to as an f-process. The former requires longitudinal optical phonons, whereas the latter requires a combination of longitudinal acoustic and transverse optical phonons.¹⁴

The effect of this additional scattering¹⁷ can be taken into consideration in a relatively simple manner as outlined by Herring. As described previously the phonons participating in this process lie near the zone boundary where the acoustic and the optical branches are either degenerate or close to each other. The average phonon energy taking part in the usual intravalley scattering (either emission or absorption) is considerably lower than that of the carriers, whereas this is not the case for phonons taking part in the intervalley scattering. In a simple model the frequency of

the phonon participating in the intervalley scattering can be approximated by an average of the transverse and acoustic mode frequencies at the zone boundary. The total relaxation time of carriers can be obtained by the addition of the inverse relaxation rates usually followed in all relaxation time approaches. Following Herring's method W_0 and W_1 are defined by the strengths of the coupling of carriers to intra- and intervalley phonons. The intervalley scattering relaxation time is then given by^{1,3,17,38}

$$\tau_w^I = \frac{W_2[(E/k\theta_0) + 1]^{1/2} + \exp(0/T)\text{Re}[(E/k\theta_0) - 1]^{1/2}}{[\exp(0/T) - 1]} \quad (30)$$

Here $\theta_0 = \hbar\omega_0/k$.

Herring calculated the temperature dependence of the mobility (μ/μ_0) vs. (T/θ_0) where $\mu_0 = \mu_0 \cdot (T/\theta_0)^{1/2}$. Using this framework and taking W_0/W_1 as an adjustable parameter the effect of the intervalley scattering can be obtained and compared with the observed values of the electronic thermal conductivity and the electrical conductivity. However, an independent determination of W_0/W_1 would be desirable.

4.4 Non-Parabolicity of the Energy Bands

Energy Dependence of the Effective Mass

In a large number of situations the energy of the carriers can be satisfactorily expressed assuming a quadratic variation with the wavevector. The simplification arises from the utilization of the first term of a more general expansion of $E(\vec{k})$. A more rigorous theoretical formulation requires the inclusion of the next higher order term in the expansion and results in a deviation from the usual parabolic relationship. The effect of this deviation becomes pronounced at high carrier densities. Moreover, narrow-band-gap semiconductors are likely to show a significant degree of non-parabolicity even at low carrier densities. Heavy doping of thermoelements makes it imperative that the effects of band non-parabolicity are taken into consideration.²⁷⁻³¹

In obtaining expressions for various transport coefficients an approach similar to the one adopted by Kane²⁸ can be considered. Defining the longitudinal and transverse components of the carrier wavevectors by k_L and k_T , it follows that:

$$\frac{k^2}{2} \frac{2k_L^2}{m_{TO}^2} + \frac{k^2}{2} \frac{k_T^2}{m_{LO}^2} = E \left(1 + \frac{E}{E_g} \right) \quad (31)$$

m_{LO}^2 and m_{TO}^2 refer to the longitudinal and transverse components of the effective mass tensor near the band extrema. The effective mass becomes energy dependent and is given by

$$m_j = m_{j0}(1 + 2E/E_g) \quad (32)$$

Effect on the Transport Coefficients

The effect of the energy dependence of the effective mass is likely to be significant in narrow-band-gap semiconductors. Expressions can be obtained for the relevant transport coefficients for a particular type of carrier scattering. Scattering by acoustic phonons is invariably present and the corresponding relaxation time which takes account of the non-parabolicity is given by³¹⁻³³

$$\tau_w^{-1} \propto [\eta(1 + \beta_L^2)]^{1/2}(1 + 2\beta_L\eta) \quad (33)$$

Here $\eta = E/kT$ is the reduced carrier energy, and $\beta_L = kT/E_g$ is the inverse of the reduced band gap. The transport coefficients can be expressed in terms of the generalized Fermi integrals defined by

$$\gamma_{Lj}^m(E, \beta_L) = \int_0^\infty \left(-\frac{\delta f}{\delta \eta} \right) \eta^m [\eta(1 + \beta_L\eta)]^m (1 + 2\beta_L\eta)^{-1} d\eta \quad (34)$$

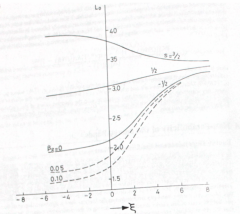


FIGURE 1. Lorenz factor L_0 plotted against reduced Fermi energy ξ for different values of the scattering parameter s . The effect of band non-parabolicity is incorporated into the calculations through the parameter β_L .

The indices n , m , l take different values for various scattering processes. The carrier concentration is given in terms of Fermi level by

$$n = \frac{(2\pi\hbar^2 kT)^{1/2}}{3\pi^2 h^3} v_{L_0}^{1/2} \quad (35)$$

The reduced electrical conductivity is given by

$$\sigma' = \frac{N\gamma T}{m_e^2 \lambda_L} v_{L_0}^{1/2} \quad (36)$$

where $\gamma = k^2 n C_{11}/(m_e^2 v_{L_0}^2)$, C_{11} and v_{L_0} refer to the longitudinal elastic constant and the deformation potential, respectively.

If one defines ' $U_1/U_{-2} = \delta$ ', the reduced Seebeck coefficient and the Lorenz factor are given by the following equations:

$$\begin{aligned} \alpha' &= [\delta(\xi) - \xi] \\ L_0 &= 2L_{-2}^{1/2} \theta_{-2}^{1/2} - \delta^2 \end{aligned} \quad (37)$$

In Figure 1 the variation of the Lorenz factor is displayed with the reduced Fermi energy for several values of the scattering parameter s corresponding to a parabolic band. The parameter β_L takes into account the effect of band non-parabolicity. Figure 2 shows the calculated variation of λ_e/λ_0 for bismuth telluride at 300 K. The calculations include the effect of non-parabolicity of the conduction band along with the intervalley scattering. The figure also displays the estimated effect

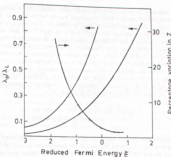


FIGURE 2 Calculated variations of λ_e/λ_h plotted against ξ in bismuth telluride at 300 K. The parameters pertain to a polycrystalline material. The effect of intervalley scattering is included ($W_2/W_1 = 0.5$). Also displayed is the effect of minority carriers. The percentage change corresponds to the estimated change corresponding to single band conduction.

of the minority carriers on the thermoelectric figure-of-merit Z . The quantity plotted is the estimated percentage change in Z if only single band conduction is taken into consideration.

4.5 Thermal Transport

A low thermal conductivity material is obviously a good choice for a thermocouple provided the power factor $a^2\sigma$ is not affected adversely. The means to achieving this have formed the central theme of most of the thermal conductivity studies in the context of thermoelectric applications.¹⁻³ The requirement of heavy doping to enhance the electrical conductivity, on the other hand, gives rise to a significant electronic contribution to the thermal conductivity. Theoretical considerations^{2,3,5,6} lead to the conclusion that higher values of Z can be obtained when $\lambda_e \sim \lambda_h$. This can be realized when the dependence of Z on the following two factors is considered: the electrical properties of the material and a degradation in performance due to parasitic heat loss.³¹ The requirement for the electronic thermal conductivity to be comparable to the lattice contribution is due to a balance in the interplay of the effectiveness of the two factors.

Several methods of obtaining a minimum in λ_h have been outlined^{6,7,36} in solid solutions, this is achieved by a selective scattering of phonons by lattice disorder, and in fine-grained materials use is made of the selective scattering of phonons by the grain-boundaries. Although there has been substantial progress in this area a significant breakthrough is unlikely, since (1) the mechanism employed to scatter phonons is likely to scatter the charge carriers, and (2) a large electronic thermal conductivity accompanies a high electrical conductivity, large λ_e , which is a necessary price to be paid. Details of the minimization of thermal conductivity is described elsewhere in the handbook.

4.6 Phonon Drag

In the theory of phonon heat transport electrons play the role of scattering centers whereas they themselves are assumed to be in equilibrium. In the same manner the photon system is assumed

to be in equilibrium while describing electronic transport even though they act as scattering agents. These assumptions are not always valid and a proper account has to be taken of the resulting "phonon drag" on electrons and "electron drag" on phonons. First proposed by Gurevich,¹⁷ a number of authors have described the drag effect in metals¹⁸⁻²¹ and laser in semiconductors.^{22,23-25} A simple treatment due to Bally²¹ is given here to illustrate the basic mechanism.

Consider phonons moving along a bar of length dx . The photon spectrum is assumed to consist of one average acoustic branch. Let $\delta N(\vec{q})$ be the number of phonons of wavevector \vec{q} that will be annihilated before reaching the cold end in order to satisfy the boundary conditions. The annihilation occurs due to the interaction with electrons by momentum-conserving or momentum-destroying processes, or by processes which do not involve electrons, such as the impurity scattering. If $\alpha'(\vec{q}; \vec{q} + \vec{G})$ is the relative probability that any one of the excess phonons will be destroyed by an Umklapp (momentum-destroying) process then

$$\alpha'(\vec{q}; \vec{q} + \vec{G}) = \frac{B(\vec{q}; \vec{q} + \vec{G})}{B_0 + \sum_{\vec{G}} B(\vec{q}; \vec{q} + \vec{G})} \quad (38)$$

B values represent absolute probabilities and B_0 refers to the sum of probabilities for all processes other than electron phonon scattering. The sum in the denominator includes all Umklapp processes in which a given change may participate. During each Umklapp process the phonons transfer a momentum $\hbar(\vec{q} + \vec{G})$ to the electron system. Thus, the probable x -component of the momentum transferred to the electronic system is

$$P_x = \delta N(\vec{q}) \alpha'(\vec{q}; \vec{q} + \vec{G}) [\hbar(\vec{q} + \vec{G})]_x \quad (39)$$

The force on the electron from phonons of wavevector \vec{q} is given by

$$F_x(\vec{q}) = \sum \frac{\delta N}{\delta x} \frac{\partial x}{\delta t} [\hbar(\vec{q} + \vec{G})] \alpha'(\vec{q}; \vec{q} + \vec{G}) \quad (40)$$

It is the time taken by the phonon of wavevector \vec{q} before being annihilated. Further,

$$\delta x(\delta t(\vec{q})) = [\nabla u(\vec{q})]_x \quad (41)$$

With the substitution $F_x = -[e] E_x N$, one obtains

$$a_x = E_x \left| \left(\frac{\delta T}{\delta x} \right) \right| = (3Ne)^{-1} \sum \alpha'(\vec{q}; \vec{q} + \vec{G}) \hbar(\vec{q} + \vec{G}) \nabla_x \omega \frac{\delta N}{\delta T} \quad (42)$$

A relatively simple calculation^{24,25} of a_x can be made at low temperatures when photon-phonon collisions are few. The photon-electron collisions are assumed to be relatively abundant. A metallic conductor is considered with a temperature gradient dT/dx . It is further assumed that the photon system behaves as a perfect gas which exerts a pressure $P = U(T)/3$ on the electron system, where $U(T)$ refers to the photon energy density. The temperature gradient gives rise to a pressure gradient, or a net directed force per unit volume, F_x , on the electrons.

$$F_x = -\frac{dP}{dx} = -\frac{1}{3} \frac{dU}{dT} \frac{dT}{dx} \quad (43)$$

The force gives rise to a current which is proportional to the temperature gradient. This is the so-called phonon drag thermoelectric current. In an open circuit an electric field E_x will be set up to balance F_x . One can write $N e E_x = F_x = 0$, N being the concentration of the conduction electrons. Further,

$$N e E_x = \frac{1}{3} \frac{dU}{dT} \frac{dT}{dx} \quad (44)$$

Defining $C_v = dU/dT$ (the lattice specific heat per unit volume)

$$\alpha_v = \frac{E_v}{dT/dx} = C_v/3Ne \quad (45)$$

The phonon drag affects both α and σ . However, the effect on σ is not as pronounced as that on α . The difference is due to the fact that the latter is a first-order effect, whereas the former is of the second order.³¹

4.7 In a Magnetic Field

Application of a magnetic field has a profound effect on the transport coefficients in addition to a wide range of galvanomagnetic and thermomagnetic phenomena.¹¹ These diverse phenomena are very useful in the understanding of the electronic structure of solids. The Lorentz force acting on an electron in a magnetic field of a few kilogauss is usually greater than the force exerted by usually attainable electric fields within the solid, and is therefore a powerful tool to probe into an electronic structure.^{11,49} The Boltzmann equation in the presence of a magnetic field now includes an extra term

$$(f'_k)_{mag} = -\frac{e}{h}(\vec{v} \times \vec{B})(\delta f_k / \delta \vec{k}) \quad (46)$$

The effect of a magnetic field is quite unlike that of an electric field. While considering the latter f'_k is substituted for f_k , giving rise to a drift which is balanced by the scattering processes. It follows that

$$e(\vec{v} \times \vec{B}) \frac{\partial f'_k}{\partial \vec{k}} = e(\vec{v} \times \vec{B}) \frac{\partial f'_k}{\partial E_k} \frac{\partial E_k}{\partial \vec{k}} = e(\vec{v} \times \vec{B}) \cdot \vec{v}_B \frac{\partial f'_k}{\partial E_k} \quad (47)$$

This obviously equals zero. The velocity vectors rotate about the field without a change in energy. The effect of the magnetic field has to be considered by considering the next term in the expansion of f_k . The magnetic field has the effect of changing the direction of motion of the electrons; it thereby acts as a sort of scattering agent. This scattering is asymmetric, being always to one side for a given field and type of carrier. In general, the effect of a magnetic field is to increase the electrical resistance. In the case of magnetoresistance the general rule is expressed as

$$\frac{\Delta \rho}{\rho_0} = F\left(\frac{B}{\rho_0}\right) \quad (48)$$

ρ_0 is the resistivity in zero field and F is a function which depends upon the material and the geometrical configuration. Obviously the magnetoresistance depends upon the relative orientation of the field and the current. Usually two configurations are considered, the transverse, when B and i are perpendicular, and the longitudinal, when they are parallel.

Bipolar effects are of importance in the context of thermomagnetic effects. In thermoelectric applications the presence of both types of carriers has to be avoided to obtain a high value for the figure-of-merit. However, the bipolar effects are not always undesirable.¹

A detailed discussion of various thermo-galvanomagnetic phenomena is available in the literature.^{50,51}

4.8 Low-Dimensional Systems

Quantum Size Effects in Two-Dimensional Systems

The study of systems that are spatially restricted in one or two dimensions has drawn a good deal of attention during recent years.⁵² When the de Broglie wavelength λ_0 of an electron is comparable

to the size of the sample, quantum size effects become important and significantly influence the transport properties. Fabrication of thin film and quantum-well-wires using advanced techniques such as MBE have made it possible to conceive devices based upon these effects. The study of electronic transport in these systems requires a knowledge of electron-scattering mechanisms. The important scattering mechanisms remain the same (acoustic and optic phonons, ionized and neutral impurities) with different energy dependences.¹¹⁻¹⁶ Once the relaxation time is known the usual Boltzmann equation approach can be followed to obtain the transport coefficients.^{11,14} The variation of the Fermi energy with carrier concentration may also be quite different and characteristic of the system considered. Model calculations based on these ideas indicate future possibilities in the context of thermoelectric applications.

A simple two-dimensional system can be considered in which electrons are confined to move in a plane. The behavior of the quasi-two-dimensional (Q2D) gas is characterized by eigenfunctions Ψ_k and energy E_k , given by

$$\Psi_k = A^{1/2} \exp[ik_x x + ik_y y] \quad (49)$$

$$E_k = \hbar^2(k_x^2 + k_y^2)/2m^* \quad (50)$$

Here $\vec{k} = (k_x, k_y)$ is a two-D vector, and A is the area of the rectangular plane of length a and breadth b . The density-of-states function $Z(\epsilon)$ is independent of the carrier energy

$$Z(\epsilon) = 2 \sum_k \delta(\epsilon - E_k) = Am^*/\pi\hbar^2 \quad (51)$$

This can be compared with the parabolic variation of the density-of-states for the bulk material. The Fermi level for the Q2D-gas is also characteristic of the system. This can be obtained from the usual normalization condition

$$\sum_k f_0(E_k) = N$$

N being the total number of electrons. The Fermi energy is given by¹¹

$$E_F = kT \ln[\exp(\pi\hbar^2 n_s / m^* kT) - 1] \quad (52)$$

where $n_s = N/a$ is the surface density of carriers.

As the density-of-states and Fermi levels are different from that of the bulk material, the transport coefficients are expected to differ. The energy dependences for the various relaxation rates are also different and thus influence the transport properties. The relaxation times for scattering by acoustic phonons and by impurities are found to be energy independent in the Q2D model considered.^{11,19}

A more realistic situation arises when the motion along the third dimension is also included, the motion being quantized in accordance with the requirements of a one-dimensional box of thickness d (between $z = 0$ and $z = d$). The eigenfunctions and eigenvalues are given by

$$\Psi = (2/\Omega)^{1/2} \exp[ik_x x + ik_y y + ik_z z] \sin(\hbar\pi z/d) \quad (53)$$

$$E = \hbar^2(k_x^2 + k_y^2)/2m^* + \hbar^2 k_z^2 / 2m^* d^2 \quad (54)$$

where $\Omega = \pi\hbar^2/2m^*d^2$.

This model gives results pertaining to a bulk gas if $d \gg D$, and the earlier simple Q2D model if $d \ll D$.

Quasi-One Dimensional Systems

Consider a gas of carriers confined to move in a long thin wire embedded in an insulating cladding. The wire may be taken to be of square cross section (sides a) and length L along the Z -direction. The eigenfunctions and eigenvalues are given by

$$\Psi_{n,l,i}(x,y,z) = \frac{2}{\sqrt{ab}} \sin(n\pi x/a) \sin(l\pi y/b) \exp(ikz) \quad (55)$$

$$E_{n,l,k} = \frac{\pi^2 h^2}{2m^*} \left(\frac{n^2 + l^2}{a^2} \right) + \hbar^2 k^2 / 2m^* \quad (56)$$

where \mathbf{k} is the electron wavevector along the z -direction.

It is of interest to consider the size-quantum limit (SQL) which assumes that all electrons are populated in the ground state ($n = n' = l = l' = 1$). This situation may arise if the wire is thin and the energy differences between sub-bands become large and the inter-sub-band transitions are not allowed in a certain temperature range. As regards the scattering one may take acoustic phonon scattering to be the dominant scattering. The energy dependence of the relaxation time is $E^{-1/2}$ instead of the usual $E^{-1/3}$ for the bulk material, and is given by⁵⁶

$$\tau_m^{-1}(\text{SQL}) = D E_g^{-3/2} \quad (57)$$

where D is a constant independent of carrier energy.

In the nondegenerate limit the Fermi energy is given by⁵⁷

$$E_F = k T \ln \left(\frac{\sqrt{2\pi mk_e \sigma^2}}{\gamma \hbar \sqrt{mkT}} \right) \quad (58)$$

where $\gamma = \sum_i \exp(-\pi^2 E_i^2 / kT)$.

$$\delta = \sum_i \exp(-l^2 E_i^2 / kT)$$

The Seebeck coefficient for the Q1D system in the SQL and nondegenerate limit is given by⁵⁷

$$\alpha^{Q1D} = \frac{k}{e} \left[2 - 1/\left(\left(\frac{2\pi}{m^* k T} \right)^{1/2} k n_e \sigma^2 \right) \right] \quad (59)$$

This can be compared with the Seebeck coefficient for the bulk material. α^{Q1D} increases with a decrease in a . For parameters pertaining to the GaAs system the results obtained by Kubakaddi and Moliman⁵⁷ show that for $a < 110$ Å at 300 K, α^{Q1D} may be greater than the corresponding bulk value.

The low-field mobility for a nondegenerate Q1D gas as obtained by Lee and Vassell⁵⁸ is given by

$$\mu = \frac{2e}{m^* k T} \sum_{n,l} \int_0^\infty dE_{nlk} E_{nlk}^{1/2} \tau(E_{nlk}) \exp(-E_{nlk}/kT) \times \\ \left[\sum_{n,l} \int dE_{nlk} E_{nlk}^{-1/2} \exp(-E_{nlk}/kT) \right]^{-1} \quad (60)$$

The mobility can be calculated as a function of temperature for various values of the dimension parameter a assuming the size-quantum limit. Calculations have also been presented for various scattering mechanisms and, over a certain range of temperature and the parameter a , the mobility is found to be greater than that for the corresponding bulk material. Figure 3 gives the variation of the mobility of a Q1D gas with temperature and the dimension parameter.

Phonon drag effects have also been discussed in low-dimensional systems by a number of workers.⁵⁹⁻⁶² The phonon drag thermopower is found to peak at a certain temperature; for AlGaAs the temperature is around 13 K.

Among the future thermoelectric materials multilayered systems utilizing the quantum-size effect are under active consideration. With advanced techniques such as molecular-beam epitaxy new exotic material systems are close to being realized in practice.

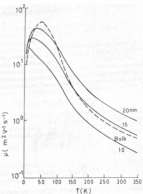


FIGURE 3 Electron mobility plotted against temperature for different values of the dimension parameter a in quasi-one-dimensional structures. The broken curve shows the three-dimensional case. (From Lee, I. and Vassell, M. O., *J. Phys. C: Solid State Phys.*, 17, 2525, 1984. With permission.)

References

- Ioffe, A. F., *Semiconductor Thermoelements and Thermoelectric Cooling*, Infosearch, London, 1957.
- Cadoff, J. R. and Miller, E., *Thermoelectric Materials and Devices*, Reinhold, New York, 1958.
- Goldsmid, H. J., *Applications of Thermoelectricity*, Methuen Monograph, London, 1960.
- Eglin, P. H., Ed., *Thermoelectricity*, John Wiley & Sons, New York, 1960.
- Ure, R. W. and Heikes, R. R., Eds., *Thermoelectricity: Science and Engineering*, Interscience, London, 1961.
- Rose, D. M. and Bhandari, C. M., *Modern Thermoelectricity*, Holt Saunders, London, 1983.
- Goldsman, H. J., *Electronic Refrigeration*, Pion Ltd., London, 1988.
- Rosi, F. D., Hockings, E. F., and Lindesblad, N. E., Semiconducting materials for thermoelectric power generation, *RCA Rev.*, 22, 82, 1961.
- Burshady, A. I., *Semicongductive Thermoelectric Devices*, Temple Press, London, 1964.
- Rosi, F. D., Thermoelectricity and thermoelectric power generation, *Solid State Electron.*, 11, 833, 1968.
- Wright, D. A., Materials for direct conversion thermoelectric generators, *Metal Rev.*, 15, 147, 1970.
- Rose, D. M., Thermoelectric power generation, *Proc. Inst. Electr. Eng.*, 125 (11R), 1113, 1978.
- Ziman, J. M., *Electrons and Phonons*, Cambridge University Press, London.
- Ridley, B. K., *Quantum Processes in Semiconductors*, Oxford University Press, New York, 1981.
- Songer, K., *Semiconductor Physics*, Springer-Verlag, Berlin, 1973.
- Bhandari, C. M. and Rose, D. M., *Thermal Conduction in Semiconductors*, Wiley Eastern Ltd., New Delhi, 1988.
- Herring, C., Transport properties of a many valley semiconductor, *Bell Systems Tech. J.*, 36, 237, 1957.

18. Long, D., Scattering of conduction electrons by lattice vibrations in silicon, *Phys. Rev.*, 120, 2024, 1960.
19. Callen, H. B., *Phys. Rev.*, 75, 1349, 1948.
20. Drabble, J. R. and Goldsmith, H. J., *Thermal Conduction in Semiconductors*, Pergamon Press, Oxford, 1961.
21. Ure, R. W., Jr., Practical limits to thermoelectric figure-of-merit II, *Energy Convers.*, 12, 45, 1972.
22. Simon, R., Thermoelectric figure-of-merit of two-band semiconductors, *J. Appl. Phys.*, 33, 1830, 1962.
23. Ritter, E. S. and Neumark, G. F., Theoretical bound on the thermoelectric figure-of-merit of two-band semiconductors, *J. Appl. Phys.*, 34, 2071, 1963.
24. Parrott, J. E., *Rev. Int. Hautes Tempér. Refract. Fr.*, 16, 393, 1979.
25. Price, P. J., Ambipolar thermopolarization of electrons and holes in semiconductors, *Philos. Mag.*, 46, 1252, 1955.
26. Bhansali, C. M. and Rose, D. M., Electronic contribution to the thermal conductivity of narrow band gap semiconductors—effect of nonparabolicity of bands, *J. Phys. D: Appl. Phys.*, 18, 873, 1985.
27. Zwanziger, W., *Adv. Phys.*, 23, 437, 1974.
28. Karz, E. O., Band structure of indium antimonide, *J. Phys. Chem. Solids*, 1, 249, 1957.
29. Ravich, Y. I., Efremova, B. A., and Tsvanachchenko, V. I., Scattering of current carriers and transport phenomena in lead chalcogenides, *Phys. Status Solidi (b)*, 43, 11, 1971.
30. Kolodziejczak, J. and Szukotypski, S., *Phys. Status Solidi*, 3, 145, 1964.
31. Ravich, Y. I., Efremova, B. A., and Smirnov, I. A., in *Semiconducting Lead Chalcogenides*, Stillman, T. S., Ed., Plenum, New York, 1970.
32. Smirnov, I. A. and Ravich, Y. I., Sov. Phys. — Semiconductors, 1, 739, 1967.
33. Rose, D. M. and Bhansali, C. M., Electronic thermal transport in thermoelectric materials—effect of band nonparabolicity, *FW International Conference on Thermoelectric Energy Conversion*, Arlington, 1986, p. 62.
34. Chatterjee, R. P. and Stratton, R. J., The thermoelectric figure-of-merit and its relation to thermoelectric generators, *J. Electron. Control*, 7, 52, 1959.
35. Goff, J. F. and Lowney, J. R., The integral formulation of the thermoelectric figure-of-merit: effect of lattice thermal conduction, 11th BEGE, p. 1561.
36. Parrott, J. E., Thermal conductivity: a guide to improved thermoelectric materials, *Proceedings of the 1st International Conference on Thermoelectrics*, 1987, p. 186.
37. Garevich, J., *Phys. USSR*, 9, 447, 1945.
38. Klemens, P. G., *Ann. J. Phys.*, 7, 528, 1954.
39. Hanna, I. I. and Sondheimer, E. H., *Proc. R. Soc. A*, 239, 247, 1957.
40. Baily, M., Transport in metals: effect of non-equilibrium phonons, *Phys. Rev.*, 112, 1587, 1958.
41. Baily, M., The phonon drag component of the thermoelectric power of the alkali metals at low temperatures, *Philos. Mag.*, 5, 1699, 1960.
42. Collins, I. G. and Ziman, J. E., *Proc. R. Soc. A*, 264, 60, 1962.
43. Frerikse, H. P. K., Thermoelectric power of Ge below room temperature, *Phys. Rev.*, 92, 248, 1953.
44. Herring, C., Theory of thermoelectric power of semiconductors, *Phys. Rev.*, 96, 1163, 1954.
45. Price, P. J., Theory of transport effects in semiconductors: thermoelectricity, *Phys. Rev.*, 104, 1223, 1956.
46. MacDonald, D. K. C., *Thermoelectricity — An Introduction to the Principles*, John Wiley & Sons, 1962.
47. Herring, C., *Proc. Int. Coll. Göttingen-Parsenkirchen*, Vieweg, Braunschweig, 1958.
48. Hartbauer, R. P., Thermoelectric power of lattice vacancies in gold, *Phys. Rev.*, 146, 502, 1966.
49. Jas, J. P., Galvanomagnetic and thermomagnetic effects in metals, *Solid State Phys.*, 5, 1, 1957.
50. Tadłowski, I. M., *Thermomagnetic Effects in Semiconductors*, Infosearch, London, 1962.
51. Purley, E. H., *The Hall Effect and Related Phenomena*, Butterworth, Sevenoaks, Kent, 1960.
52. Ando, T. and Mori, S., Electronic properties of a semiconductor superlattice, *J. Phys. Soc. Jpn.*, 47, 1518, 1979.
53. Arosa, V. K. and Awad, F. G., Quantum size effects in semiconductor transport, *Phys. Rev. B*, 27, 5570, 1981.
54. Ridley, B. K., *J. Phys. C: Solid State Phys.*, 15, 5899, 1982.
55. Lee, J. and Spector, H. N., *J. Appl. Phys.*, 54, 3299, 1983.

56. Lee, J. and Vassil, M. G., Low-field electron transport in quasi-one dimensional semiconducting structure, *J. Phys. C: Solid State Phys.*, 17, 2525, 1984.
57. Kabakadli, S. S. and Moshnai, R. G., Thermopower enhancement in semiconducting quantum-well wires for acoustic phonon scattering, *J. Appl. Phys.*, 58(9), 3643, 1985.
58. Keerney, M. I. and Butcher, P. N., A calculation of the effect of sub-band structure of the thermopower of a quasi-one-dimensional wire, *J. Phys. C: Solid State Phys.*, 19, 5429, 1986.
59. Kawai, S., *J. Phys. Soc. Jpn.*, 27, 906, 1969.
60. Nicholas, R. J., *J. Phys. C: Solid State Phys.*, 18, L685, 1985.
61. Fletcher, R., Mann, J. C., and Weissman, G., Experimental results on the high field thermopower of a two-dimensional electron gas in a GaAs-Ga_{1-x}Al_xAs heterojunction, *Phys. Rev. B*, 32, 8477.
62. Castrell, D. G. and Butcher, P. N., A calculation of the phonon-drag contribution to thermoelectric power in two-dimensional systems, *J. Phys. C: Solid State Phys.*, 19, L429, 1986.

5

Optimization of Carrier Concentration

C. M. Bhandari
University of Allahabad
India

David M. Rowe
University of Wales,
Cardiff, U.K.

5.1 Introduction	43
5.2 Single Band Conduction	43
Classical Statistics • Optimum Fermi Level • Optimum Seebeck Coefficient • Fermi-Dosov Statistics	
5.3 Two-Band Conduction	47
Idealized Models • Realistic Situations	
5.4 Further Considerations	48
Multivolley Structure with Intervalley Scattering • Non-Parabolic Energy Bands	
5.5 Improved Materials	49
Optimum Carrier Concentration • Dopant Precipitation and Solubility • New Materials	
References	51

5.1 Introduction

The thermoelectric figure-of-merit is defined by $Z = \alpha^2\sigma/k$ where α , σ , and k refer to the Seebeck coefficient, electrical conductivity, and the thermal conductivity of the thermoelectric material. This parameter is of central importance in any program to optimize the thermoelectric properties.¹⁻³ The Seebeck coefficient and electrical conductivity depend strongly on the Fermi level^{4,5,14,15} which in turn depends upon the carrier concentration, the carrier effective mass, and the temperature. In theoretical formulations it is convenient to express the thermoelectric transport coefficients in terms of the Fermi energy E_F (conventionally measured from the band edges). Since the thermal conductivity depends only weakly on the carrier concentration (n) the general effect of an increase in carrier concentration would manifest itself in the figure-of-merit, through the power factor $n^2\sigma$ (Figure 1).

5.2 Single Band Conduction

Classical Statistics

It is convenient to start from simple theoretical considerations and then gradually develop more refined models. Consider a single band (either an electron or hole band) with the usual parabolic density-of-states distribution and assume that the carriers obey classical statistics. The Seebeck coefficient¹ can be expressed as

$$\alpha = \mp \frac{k}{e} (5/2 + s - \xi) \quad (1)$$

The signs \mp refer to the contributions from electrons and holes, respectively. $\xi = (E_0/kT)$ is the reduced Fermi energy, k is the Boltzmann's constant, T the absolute temperature, s refers to the

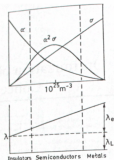


FIGURE 1 Dependence of α , σ , λ , and $n^2\sigma$ on the concentration of free carriers (schematic).

scattering parameter, and it is assumed that the carrier relaxation time can be expressed in terms of the carrier energy in a simple way, i.e., τ is proportional to E .

The electrical conductivity is given by

$$\sigma = n\mu_e E \quad (2)$$

where μ_e is the carrier mobility in the low carrier concentration limit. The carrier concentration is related to the reduced Fermi energy by the equation

$$n = (2\pi m^* kT/h^2)^{1/2} \exp \xi \quad (3)$$

The thermal conductivity is written as a sum of the lattice and the electronic components, i.e., $\lambda = \lambda_L + \lambda_e$. Evidently ξ affects the thermal conductivity only through the electronic contribution λ_e .

In addition $\lambda_e = L_e (kT)^2 \sigma T$, where the dimensionless quality L_e is referred to as the Lorenz factor. In the limit of low carrier concentration it can be shown^{1,2} that $L_e = (5/2 + s)$. When the following parameters are introduced:

$$F = \frac{\mu_e}{\lambda_L} \left(\frac{m^*}{m} \right)^{1/2} \quad (4)$$

$$G = (2\pi m k T / h^2)^{1/2}$$

the thermoelectric figure-of-merit can, after some rearrangement, be expressed as

$$Z = (5/2 + s - (\xi^2) \left[2 \frac{k^2}{e} F G \exp \xi \right]^{-1} + (5/2 + s) T] \quad (5)$$

Optimum Fermi Level

The figure-of-merit varies with the Fermi level and the optimum value of ξ which maximizes Z is obtained by setting $dZ/d\xi = 0$. This gives³

$$\xi_{opt} + 4(5/2 + s)\frac{k^2}{e}FGT\exp\xi_{opt} = \frac{1}{2} + s \quad (6)$$

In general, the lattice contribution to the thermal conductivity is large. Neglecting the second term in Equation 6, which amounts to neglecting k_e , gives:

$$\xi_{opt} = s + \frac{1}{2} \quad (7)$$

When the electron scattering is by acoustic phonons and ionized impurities the scattering parameter s takes values of $-1/2$ and $+3/2$, respectively, with corresponding ξ_{opt} values of 0 and 2. Including the electronic thermal conductivity will amount to a reduction in ξ_{opt} . Obviously, the thermoelectric material has to be doped heavily to obtain Fermi levels well within the bands. Corresponding values of the optimum carrier concentrations can be estimated from Equation 3.

Optimum Seebeck Coefficient

An estimate¹⁴ for the optimum Seebeck coefficient that maximizes Z can be obtained by differentiating Z with respect to θ at constant temperature and equating $dZ/d\theta$ to zero. Classical statistics gives $d(\log \alpha)/d\theta = e\kappa$, for all scattering mechanisms. Consequently,

$$\alpha_{opt} = -2\frac{k}{e}[1 + (\lambda_e/\lambda_L)] = -172[1 + (\lambda_e/\lambda_L)] \mu V/K \quad (8)$$

In this model higher values for Z_{max} are obtained^{15,16} when $\lambda_e/\lambda_L = 0.5$, $\alpha_{opt} = 250 \mu V/K$, $Z_{max}T = 4/1_{av}$. In the case of acoustic phonon scattering $Z_{max}T = 2$.

The results predicted by this simple model are not unrealistic. A more rigorous theoretical model can be formulated which takes into account several important features that characterize a thermoelectric semiconductor,^{6,7,17,18} viz., the presence of several equivalent valleys in the conducting band, with or without intervalley electron scattering, minority carrier effects, and possible deviations from the parabolic $E-k$ relationship.

Fermi-Dirac Statistics

The use of classical statistics in describing the behavior of the carriers is justified only in the limit of low carrier concentration. As the thermoelectric material is heavily doped, Fermi-Dirac statistics must be employed. The expressions for the Seebeck coefficient and the Lorenz factor then take the form^{1,6}

$$\alpha = \mp \frac{k}{e}(\bar{\delta} - \xi) \quad (9)$$

where

$$\bar{\delta} = \frac{(s + 5/2)F_{1/2}(E)}{(s + 3/2)F_{3/2}(E)} \quad (10)$$

and

$$L_{av} = \frac{(s + 7/2)F_{1/2}(E)}{(s + 3/2)F_{3/2}(E)} - \bar{\delta}^2 \quad (11)$$

$F_i(E)$ are the Fermi integrals.

The electrical conductivity is given by $\sigma = \sigma_0 \epsilon$, where

$$\sigma_0 = 2(2\pi m^* k T/h^2)^{1/2} e \mu \quad (12)$$

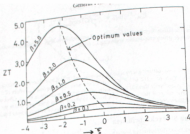


FIGURE 2. Dimensionless figure-of-merit (ZT) plotted against reduced Fermi energy (ξ) for $s = -1/2$. (From Chaiken, R. P. and Stratton, R. I., J. Electron. Control, 7, 53; 1959. With permission.)

and

$$\epsilon = F_{s+1/2}(\xi)(s + 1/2)! \quad (13)$$

These equations enable the dimensionless thermoelectric figure-of-merit to be expressed as

$$ZT = (\bar{\beta} - \xi)^2 \left[\frac{1}{L_0} + \left(\frac{\sigma}{\lambda_L} T k/e^2 \right)^2 \right]^{-1} \quad (14)$$

It is convenient to work with the dimensionless quantity, σ' , referred to as the reduced electrical conductivity, where

$$\sigma' = (\sigma/\lambda_L) T (k/e^2)^2 \quad (15)$$

The dimensionless figure-of-merit is then given by⁴

$$ZT = \frac{(\bar{\beta} - \xi)^2}{L_0 + 1/\sigma'} \quad (16)$$

In addition

$$\sigma' = \beta F_{s+1/2}(\xi)/(s + 1/2)! \quad (17)$$

with

$$\bar{\beta} = \frac{2(2\pi k)^{3/2} k^2}{e h^5} A' \quad (18)$$

$$A' = T^{3/2} m^{1/2} \mu/h_L \quad (19)$$

The dependence of the Fermi level on carrier concentration is now given by

$$n = \frac{4}{\sqrt{\pi}} (2\pi m^* k T)^{1/2} F_{1/2}(\xi) \quad (20)$$

The parameters A' and $\bar{\beta}$, which make their appearance in the expression for the figure-of-merit, are referred to as the material parameters, since for a given scattering mechanism and Fermi level, the figure-of-merit depends on the physical properties of the material only through these parameters. A plot of ZT vs. ξ for scattering by acoustic phonons is displayed in Figure 2.

5.3 Two-Band Conduction

Idealized Models

Although the materials are heavily doped by the addition of n- or p-type impurities, the presence of the second band and the inevitable presence of minority carriers have a significant effect on the thermoelectric properties. Narrow-band-gap semiconductors are usually good thermoelectric materials and are quite likely to exhibit the minority carrier effects at the upper end of their temperature ranges of operation. Following Ritter and Neusmark²⁰ an insight into the conditions that favor a high figure-of-merit can be obtained for a simple two-band model¹⁹⁻²² of a semiconductor with several equivalent extrema in its conduction or valence bands.^{21,18,21} The lattice contribution to the thermal conductivity is neglected in these considerations.

The conduction and valence bands are considered as having N_e and N_h equivalent extrema (or valleys), respectively. If σ_v represents the contribution of a single valley to the electrical conductivity, then:

$$\sigma_{e,h} = N_{e,h} \sigma_{v,e,h} \quad (21)$$

where the suffices e and h refer to the electron and hole contributions from the two bands. The total electrical conductivity is a sum of the contributions from the two bands, i.e., σ = σ_e + σ_h. Also, the Seebeck coefficient appropriate to a two-band conduction model is written as

$$\alpha = (\alpha_e \sigma_e + \alpha_h \sigma_h) / (\sigma_e + \sigma_h) \quad (22)$$

The total Seebeck coefficient is then given by²⁰

$$\alpha = \frac{k}{e} \left[-\frac{(\xi_e - \xi_v)}{1 + \sigma_v/\sigma_e} + \frac{(\xi_h - \xi_v)}{1 + \sigma_e/\sigma_h} \right] \quad (23)$$

and the ratio σ_e/σ_h by

$$\sigma_e/\sigma_h = \gamma^2 [F_{N_{e+1}}(\xi_v)]/[(\xi_v + 1/2)] / [F_{N_{h+1}}(\xi_v)]/[(\xi_v + 1/2)] \quad (24)$$

where suffices v and h refer to the scattering parameters for the electron and hole systems, respectively. The density-of-states effective masses for electrons and holes are given as

$$m^* = N^{2/3}(m_1 m_2 m_3)^{1/3} \quad (25)$$

where m₁, m₂, and m₃ are mass components along principal axes. N refers to the number of equivalent valleys in the band (N_e or N_h). If the parameter γ is taken to be the same for the two bands, and classical statistics is used, then

$$A = [s + 5/2 - \xi] \quad (26)$$

$$L_s = s + 5/2 \quad (27)$$

and

$$\sigma_e/\sigma_h = \gamma^2 \exp(\xi_v + 2\xi) \quad (28)$$

Here ξ_v = E_v/kT is the dimensionless energy band gap. In the present model ξ_v/σT is independent of ξ_v (ξ_v) and γ and a variation in these parameters will affect Z only through σ. It is therefore sufficient to consider the dependence of α on these parameters, which yields the following

$$\alpha = \frac{k}{e} [-M \tanh \xi' + \xi' - 1/\gamma] \quad (29)$$

where ξ' = ξ + ξ_v/2 + 1/γ and M = s + 5/2 + ξ_v/2.

For a given γ, the optimum Fermi level corresponding to a maximum Z is given by

$$\begin{aligned} \xi_{opt} &= -\xi_v/2 + 1n[\sqrt{M} + \sqrt{M - 1}] - 1/\gamma, \text{ for } \xi' > 0 \\ &= -\xi_v/2 - 1n[\sqrt{M} + \sqrt{M - 1}] - 1/\gamma, \text{ if } \xi' < 0 \end{aligned} \quad (30)$$

A detailed study of the conditions under which the upper bound on Z can be raised reveals that the parameter γ is of central importance.¹⁰ The model predicts a large value of Z for high values of m_e^*/m_h^* and m_h^*/m_e^* . These results pertain to a highly simplified model and cannot be applied, in such, to realistic situations. However, they do point towards possible directions in which to look for future developments.

Realistic Situations

Simon¹¹ has outlined a procedure which provides a reasonable estimate of Z_{\max} (i.e., Z at the optimum carrier concentration) from the measured values of α , σ , and k on a sample which is not too heavily doped. Implicit in the procedure is the assumption that the scattering parameter s is independent of δ , an assumption invariably present in most calculations. When more than one scattering mechanism operates simultaneously a mixed scattering model has to be adopted.¹²

In practical situations a two-band conduction model can be considered and appropriate parameters selected from among the known thermoelectric materials. The maximization of Z can then be considered with respect to variations in δ . The bipolar contribution to the thermal conductivity is included and is given by

$$\lambda_b = T \left(\frac{k}{e} \right)^2 \frac{\sigma_v \sigma_b}{\sigma_v + \sigma_b} |\delta_v + \delta_b + \xi_g|^2 \quad (31)$$

Using this model the dimensionless figure-of-merit is written as¹²

$$ZT = \frac{(\alpha'_v \alpha'_b - \alpha'_v \sigma'_b)^2}{(\sigma'_v + \sigma'_b)(1 + \sigma'_v L_{\text{low}} + \sigma'_b L_{\text{high}} + \sigma'_v \sigma'_b (\delta_v + \delta_b + \xi_g))^2} \quad (32)$$

Urn¹³ used these equations and optimized Z with respect to variations in δ . He selected various parameters, such as the effective mass and the elastic constant, from among the best-known thermoelectric materials. Urn's result slightly overestimates Z , but the calculation can be made more rigorous by choosing all the relevant parameters from a particular material.

This formulation can yield valuable information about the effect of minority carriers on various transport coefficients. Z may change considerably due to the effect of the second band as a result of the contributions to α and σ , and also through the thermal conductivity which now includes a contribution due to electron-hole pairs. These aspects have been discussed in detail for bismuth telluride.¹⁴

Goff and Lowsey¹⁵ reformulated ZT in integral form and used it to analyze the thermoelectric behavior of lead telluride. The analysis emphasizes the effect of changing the values of internal parameters arbitrarily. As expected, setting $\lambda_b = 0$, for example, increases ZT . In this case the lower carrier concentrations yield larger Z , unlike the normal situation (i.e., with normal values of λ_b), where larger carrier concentrations correspond to larger ZT . Nevertheless such considerations can be helpful in material development programs.

5.4 Further Considerations

Multivalley Structure with Intervalley Scattering

It has often been emphasized that the presence of a number of equivalent valleys in the bands has the effect of increasing the figure-of-merit, provided, of course, that the scattering of carriers between different valleys can be avoided.^{16,17,27} For such scattering to take place high-energy photons are required and these may not be available in sufficient numbers at low temperatures. At elevated temperatures the intervalley scattering of carriers may partly offset²⁷ the gain in the figure-of-merit.

Non-Parabolic Energy Bands

Another unavoidable complication arises due to the deviation from the parabolic energy-wave-vector relationship.²⁸⁻³² In obtaining the transport coefficients for non-parabolic bands an approach is usually employed which takes account of the electron energy dispersion:^{21,28,31}

$$\frac{\hbar^2}{2} \frac{2k_L^2}{m_{L0}^*} + \frac{\hbar^2}{2} \frac{k_T^2}{m_{T0}^*} = E \left(1 + \frac{E}{E_g} \right) \quad (33)$$

where k_L and k_T are the longitudinal and transverse components of the electron (or hole) wave-vector and m_{L0}^* and m_{T0}^* are the components of the effective mass tensor near the band extrema. The effective mass now becomes energy dependent, with

$$m_j^* = m_{j0}^* (1 + 2\eta \beta_j) \quad (34)$$

where $\beta_j = E_g^{-1}$ is the inverse of the energy band gap, and $\eta = E/kT$ is the reduced carrier energy. For large band gaps $\beta_j \ll 1$ and the effective mass take a constant value as in parabolic bands. The calculated transport coefficients based on these considerations are significantly different in narrow-band-gap semiconductors; the Lorenz factor and electrical conductivity are reduced compared to values obtained using the parabolic model.

Burdette and Rowe have taken these aspects into consideration and obtained estimates for the possible effects of valleys with and without additional scattering, and deviations from band parabolicity.^{29,30} This model can be used in analyzing known data as well as in investigating the role of various parameters in enhancing the figure-of-merit. The power factor $\alpha^2\sigma$ is of prime importance when optimizing with respect to E . Situations can also be considered in which the number of valleys is increased while the other parameters are fixed. Studies of the silicon-germanium system indicate that $\alpha^2\sigma$ (max) increases by a factor slightly less than N_v in the absence of intervalley scattering. This sets an upper limit on the increase in Z due to the number of valleys. Interestingly n_{opt} also exhibits a corresponding increase. In a "model calculation" based on the Si_{0.9}Ge_{0.1} system at room temperature a sixfold increase in N_v has the effect of multiplying $\alpha^2\sigma$ by a factor of 5.0, whereas n_{opt} is multiplied by a factor of 6.2. For $N_v = 6$, pertaining to the situation in silicon, $n_{opt} \sim 2.5 \times 10^{17} \text{ m}^{-3}$. It is important, of course, to note that to take maximum advantage of these considerations n_{opt} should stay well below the solubility limit.

5.5 Improved Materials

Optimum Carrier Concentration

The introduction of "additives" may enhance the thermoelectric performance of a material, as has been reported for silicon-germanium. Significant improvements in the figure-of-merit accompany the addition of gallium phosphide to the silicon-germanium system.³¹⁻³⁴ This increase appears primarily due to an increase of $\alpha^2\sigma$; and in particular due to an increase in σ . The mechanism for the phenomenon is not well understood and there have been various investigations to identify it.^{34,35} High-temperature annealing is found to have a profound effect on the reported increase in performance. Normally the maximum figure-of-merit occurs at concentrations that are not normally attainable in practice, as is the case with silicon-germanium. The introduction of gallium phosphide followed by annealing appears to raise the dopant solubility limit and is accompanied by an increase in $\alpha^2\sigma$. For standard Si_{0.9}Ge_{0.1} samples the optimum carrier concentration is around $(1.4 - 1.8) \times 10^{16} \text{ m}^{-3}$, whereas for silicon-germanium alloys to which gallium phosphide has been added it is found to be around $2.2 \times 10^{16} \text{ m}^{-3}$. It should be pointed out that the Seebeck coefficient is not expected to change significantly as it depends on $\log n$. Hall effect measurements appear to confirm this.

The above explanation appears reasonable but it cannot possibly account for the reported magnitude of increase in the figure-of-merit. Theoretical estimates based on fairly rigorous calculations^{30,39} can be employed in assessing the possible increase in the figure-of-merit which

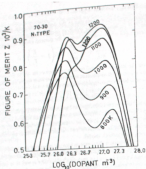


FIGURE 3. Z vs. dopant concentration for n -type samples of $\text{Si}_{0.7}\text{Ge}_{0.3}$ $m^4(L)/m_e = 2$, where L refers to the L-band; k_b obtained from the measured k . (From Slack, G. A. and Hassain, M. A., *J. Appl. Phys.*, 70(5), 2694, 1991. With permission.)

accompanies an increase in carrier concentration. In the case of $\text{Si}_{0.7}\text{Ge}_{0.3}$ alloy a plot of $\alpha^2 \sigma$ vs. n at 300 K shows a 12.5% rise in the power factor when n increases by a factor of 1.6 just before the maximum. This is about half the reported increase in the figure-of-merit in silicon-germanium gallium phosphide annealed samples. The effect of heat treatment on the electrical power factor is not yet fully understood, neither is the reported (almost unchanged) thermal conductivity. At these high doping levels the electronic contribution is not negligible and changes in the electrical conductivity should be reflected in a change in the electronic thermal conductivity. Microstructure studies by scanning electron microscopy have revealed the presence of new phases. This has been particularly important in other high-temperature materials, such as the lanthanum chalcogenides La_xTe_y with $0 < x < 1/3$; these are among the best-known high-temperature thermoelectric materials with the figure-of-merit showing a maximum around a temperature of 1273 K. However, even similar samples appear to behave differently. Microscopic examination of the material reveals¹⁶ new phases and structures which are dependent on the methods and processes used in chemically synthesizing the compound and subsequent hot-pressing. The presence of oxy-telluride phases have been reported indicating the possibility of varying degrees of oxygen contamination. It is relevant to any clear understanding of the sample behavior that the sample history is known, including any previous thermal annealing. Slack and Hassain's¹⁶ analysis of the thermoelectric behavior of the silicon-germanium system does not support the reported effectiveness of Ga⁺ doping and grain-boundary scattering in enhancing the figure-of-merit. Using a model with one valence and two conduction bands they obtained the dependence of the figure-of-merit on carrier concentration at several temperatures (900 to 1300 K), as shown in Figure 3. The curves show two distinct maxima, the left one (at lower n) being usually higher than the other. However, above 1130 K the maximum figure-of-merit shifts to the right side, and n_{opt} is around 10^{17} m^{-3} . This is somewhat higher than other reported values of n_{opt} .¹⁸ These calculations, however, neglect the non-parabolic nature of the energy bands and intervalley scattering, both of which may be significant at the doping levels and temperatures considered.

Dopant Precipitation and Solubility

Often in thermoelectric semiconductors, the dopants possess retrograde characteristics which are strongly temperature dependent⁴² and the dopant concentration may well exceed the solubility limit.⁴³ This can considerably influence the material's properties when operated over a period of time. For example, the effect of phosphorus precipitation on the room temperature Seebeck coefficient of $\text{Si}_{0.7}\text{Ge}_{0.3}$ alloy⁴⁴ shows that the precipitation is very fast over the temperature range 700 to 800 K, with the carrier concentration decreasing by around 50% after only 1 s. However, the process is reversible and suitable annealing procedures may redissolve the dopant. The precipitation of boron is slower than that of phosphorus and is fastest in the range 1000 to 1200 K. A theoretical analysis of the dopant precipitation has been provided by the Lifshitz-Slyozov model,⁴⁵ and the long-term behavior of the material can be predicted from the results of relatively short-term heat treatment.⁴⁶

As regards the dopant solubility the mechanism is not difficult to understand when both n- and p-type impurities are present. Considering the reaction



it can be seen that the formation of electron-hole pairs ($e^+ e^-$) depletes the solution of electrons, and consequently more donors are ionized leading to a greater solubility. The effectiveness of the process depends upon the degree of dissociation of electron-hole pairs. Studies on the solubility of lithium in germanium show that the presence of gallium considerably increases the lithium solubility.⁴⁷ For example, the concentration of lithium in pure germanium at room temperature goes up from its normal value of 10^{10} m^{-3} to about 10^{11} m^{-3} when doped with gallium. However, these considerations must be investigated much more comprehensively before a quantitative understanding can be achieved of the reported increase in the figure-of-merit.

New Materials

Recent advances in new materials must include a mention of the low dimensional systems⁴⁸⁻⁵¹ — thin films and micro-thin wires operating in the size-quantum limit. The mobility and the Seebeck coefficient in these systems may be favorably influenced in a particular temperature range and for a certain range of film thicknesses. Advanced preparation techniques like molecular beam epitaxy can be used to prepare exotic new material structures, such as synthetic superlattices and the strained-layer heterostructures. The figure-of-merit may be increased by these and other factors, such as the effect of strain on the phonon properties, electrical conductivity enhancement by modulation doping, and carrier confinement in quantum wells. The carrier densities pertaining to the onset of degeneracy in these systems may be lower than that in the bulk and this may have some relevance in achieving optimization of the carrier concentration.

References

1. Ioffe, A. F., *Semiconductor Thermoelements and Thermoelectric Cooling*, InstiSearch, London, 1957.
2. Cadoff, I. B. and Miller, E., *Thermoelectric Materials and Devices*, Reinhold, New York, 1959.
3. Goldsmid, H. J., *Applications of Thermoelectricity*, Methuen Monograph, London, 1960.
4. Egli, P. H., Ed., *Thermoelectricity*, John Wiley & Sons, New York, 1960.
5. Uso, R. W. and Heikes, R. R., Ed., *Thermoelectricity: Science and Engineering*, Interscience, London, 1961.
6. Rowe, D. M. and Bhandari, C. M., *Modern Thermoelectrics*, Holt Saunders, London, 1983.
7. Goldsmid, H. J., *Electroic Refrigeration*, Pion Ltd., London, 1988.
8. Rossi, F. D., Hoekings, E. F., and Lindenblad, N. E., Semiconducting materials for thermoelectric power generation, *RCA Rev.*, 22, 82, 1961.
9. Barshay, A. I., *Semiconductor Thermoelectric Device*, Temple Press, London, 1964.
10. Rossi, F. D., Thermoelectricity and thermoelectric power generation, *Solid State Electron.*, 11, 833 1968.

11. Wright, D. A., Materials for direct conversion of thermoelectric generators, *Metal. Rev.*, 15, 147, 1970.
12. Rose, D. M., Thermoelectric power generation, *Proc. Inst. Electr. Eng.*, 125(11R), 1113, 1978.
13. Bhandari, C. M. and Rose, D. M., Silicon-germanium alloys as high temperature thermoelectric materials, *Commun. Phys.*, 10(5), 219, 1988.
14. Hunsur, R. A., Ritter, E. S., and DuPre, F. K., Fermi levels in semiconductors, *Philips Res. Rep.*, 5, 188, 1950.
15. Fatali, V. L., *Hemispherical Semiconductors*, Plenum, New York, 1968.
16. Chauhan, R. P. and Stratton, R. J., The thermoelectric figure of merit and its relation to thermoelectric generators, *J. Electron. Control.*, 7, 52, 1958.
17. Ziman, J. M., *Electrons and Phonons*, Cambridge University Press, London, 1960.
18. Ridley, B. K., *Quantum Processes in Semiconductors*, Oxford University Press, New York, 1981.
19. Simon, R., Thermoelectric figure-of-merit of two-band semiconductors, *J. Appl. Phys.*, 33, 1830, 1962.
20. Ritter, E. S. and Neimark, G. F., Theoretical bound on the thermoelectric figure-of-merit of two-band semiconductors, *J. Appl. Phys.*, 34, 2071, 1963.
21. Bhandari, C. M. and Rose, D. M., *Thermal Conduction in Semiconductors*, Wiley Eastern Ltd., New Delhi, 1988.
22. Uva, R. W., Jr., Practical limits to the thermoelectric figure-of-merit. II, *Energy Convers.*, 12, 45, 1972.
23. Bhandari, C. M. and Rose, D. M., Minority carrier effects on thermoelectric figure-of-merit, *Proceedings of the 1st European Conference on Thermoelectrics*, Cardiff, 1987, p. 178.
24. Goff, J. F. and Lowrey, J. R., The integral formulation of the thermoelectric figure of merit: effect of lattice thermal conduction, *Proceedings of the 11th IECEC*, 1976, p. 1561.
25. Hastings, C., Transport properties of a many valley semiconductor, *Bell Systems Tech. J.*, 34, 237, 1955.
26. Seeger, R., *Semiconductor Physics*, Springer-Verlag, Berlin, 1975.
27. Bhandari, C. M. and Rose, D. M., The behaviour of a multivalley semiconductor, *Proceedings of the VIIth International Conference on Thermoelectric Energy Conversion*, Arlington, 1984, p. 38.
28. Kane, E. O., Band structure of $lnSb$, *J. Phys. Chem. Solids*, 1, 249, 1957.
29. Rose, D. M. and Bhandari, C. M., Electronic thermal transport in thermoelectric materials — effect of band non-parabolicity, *Proceedings of the VIIth International Conference on Thermoelectric Energy Conversion*, Arlington, 1984, p. 62.
30. Bhandari, C. M. and Rose, D. M., Electronic contribution to the thermal conductivity of narrow band gap semiconductors — effect of non-parabolicity of bands, *J. Phys. D: Appl. Phys.*, 18, 873, 1985.
31. Ravich, Y. I., Efimova, B. A., and Savinov, I. A., *Semiconducting Lead Chalcogenides*, St. Ioffe, T. S., Ed., Pergamon, New York, 1978.
32. Ravich, Y. I., Efimova, B. A., and Tamarchenko, V. I., *Phys. Status Solidi (b)*, 43, 11, 1971.
33. Rose, D. M. and Bhandari, C. M., A review of lead telluride technology at UWIST, *Sixth International Conference on Thermoelectric Energy Conversion*, Arlington, 1986, p. 43.
34. Bhandari, C. M. and Rose, D. M., unpublished.
35. Fisherdyke, R. K. and Garvey, L. P., Modified Si-Ge alloys with improved performance, *Proc. 13th IECEC*, 3, 1983, 1978.
36. Vining, C., personal communication.
37. Vanderschueren, J. W., Wood, C., and Draper, S., *Proc. Spring Meet. Mater. Res. Soc.*, Anaheim, CA, 1987, p. 21.
38. Wood, C., Materials problems in high temperature thermoelectric energy conversion, *1st European Conference on Thermoelectrics*, Cardiff, 1987, p. 1.
39. Rose, D. M., Mit, G., and Bhandari, C. M., The effect of high temperature heat treatment on the electrical power factor of Si-Ge/Ga₂ alloy, *Proc. 2nd Asian Thermophys. Prep. Conf.*, 1989, p. 145
40. Slack, G. A. and Hussain, M. A., The maximum possible conversion efficiency of Si-Ge thermoelectric generators, *J. Appl. Phys.*, 70(5), 2694, 1991.
41. Trumbore, F. A., Solid solubilities of impurity elements in Ge and Si, *Bell Systems Tech. J.*, 39, 265, 1960.

42. Ekstrom, L. and Diamokas, J. P., Precipitation of phosphorus from solid solution in Ge-Si alloys, *J. Phys. Chem. Solids*, 857, 1966.
43. Savvidis, N. and Rowe, D. M., Precipitation of phosphorus from solid solution of Si-Ge alloys and its effect on thermoelectric transport properties, *J. Phys. D: Appl. Phys.*, 14, 723, 1981.
44. Lifshitz, I. M. and Slyozov, V. V., *J. Phys. Chem. Solids*, 19, 35, 1961.
45. Raag, V., Comprehensive thermoelectric properties of n and p-type $\text{Si}_x\text{Ge}_{1-x}$, *Proc. 2nd Int. Conf. Thermoelectric Energy Conversion*, Arlington, 1978, p. 5.
46. Glazov, V. M. and Zemskov, V. S., *Physicochemical Foundation of Semiconductor Doping*, Narva, Moscow, 1967.
47. Ando, T. and Mori, S., Electronic properties of a semiconductor superlattice. I. Self-consistent calculation of subband structure, *J. Phys. Soc. Jpn.*, 47, 1518, 1979.
48. Areotis, V. K. and Awad, F. G., Quantum size effects in semiconductor transport, *Phys. Rev. B*, 23, 5570, 1981.
49. Ridley, B. K., *J. Phys. C: Solid State Phys.*, 15, 5899, 1982.
50. Lee, I. and Spector, H. N., *J. Appl. Phys.*, 54, 3291, 1983.
51. Lee, J. and Vassell, M. O., Low-field electron transport in quasi-one-dimensional semiconducting structures, *J. Phys. C: Solid State Phys.*, 17, 2525, 1984.
52. Kubakaddi, S. S. and Mulimari, B. G., Thermopower enhancement in semiconducting quantum-well wires for acoustic phonon scattering, *J. Appl. Phys.*, 58(9), 3643, 1985.
53. Whall, T. E. and Parker, E. H. C., Preparation of advanced materials by MBE, 1st European Conf. on Thermoelectrics, Cardiff, 1987, p. 51.

6

Minimizing the Thermal Conductivity

C. M. Bhandari
University of Allahabad
India

6.1 Introduction	55
6.2 Requirement of Low Thermal Conductivity	56
6.3 Reducing the Lattice Thermal Conductivity	57
Alloy Disorder • Raman Scattering • Scattering by Charge Carriers • Scattering by Grain Boundaries	
6.4 Fine-Grained Materials	61
Improving the Ratio of Electrical to Thermal Conductivity • Other Considerations	
6.5 Towards a Minimum Thermal Conductivity	63
References	63

6.1 Introduction

The study of heat transport^{1–5} in semiconductors requires a knowledge of a number of material properties. On the other hand, heat transport studies can yield useful information on several of these properties. In addition to this, a knowledge of the thermal conductivity and the means by which it can be increased or decreased in a selective manner is of considerable practical importance.⁶

The thermoelectric performance^{6–10} of a material is characterized by the so-called figure-of-merit $\alpha^2\sigma/k$, where α , σ , and k refer to the Seebeck coefficient and the electrical and thermal conductivity of the material, respectively. The thermal conductivity of a semiconductor has two main components: the lattice (phonon) component (k_L), and the electronic (or hole) component (k_e). The electronic thermal conductivity is written as

$$k_e = \left(\frac{k}{e} \right)^2 L_0 \sigma T \quad (1)$$

In semiconductors the Lorenz factor L_0 varies with the level of doping. This is discussed in terms of the Fermi level, which relates to the energy E_F measured from the band edge. It is convenient to introduce a reduced Fermi energy $\xi = E_F/kT$, and reduced energy band gap $\xi_0/kT = 1/\beta_0$; the Lorenz factor in a semiconductor depends upon ξ , β_0 , and the particular carrier scattering mechanism. The variation of L_0 with β_0 incorporates into the calculation the influence of the second band, which manifests itself in deviations from the parabolic energy-wavevector relationships.^{5,11,12} The Lorenz factor can be calculated as a function of ξ and β_0 , with the latter taking account of the non-parabolicity of the energy bands. For the usual parabolic band model a relaxation time τ can be defined for the carriers which varies as E^γ , where E refers to the carrier energy. The scattering parameter s takes on different values for different scattering mechanisms. The figure-of-merit can be optimized with respect to the variation of ξ , and its optimum value is given by $\xi_{opt} = 1/2 + s$. In a simple theoretical framework the figure-of-merit is expressed in terms of various parameters and maximizes with respect to variations in α , yielding¹¹

$$\alpha_{opt} = -2\frac{k}{e}[1 + (\lambda_e/k_L)] \quad (2)$$

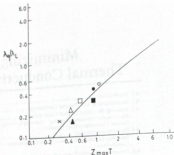


FIGURE 1 Maximum dimensionless figure-of-merit for several thermoelectric materials plotted against the ratio λ_0/k_L at 300 K. (□) p-type Sb₂Te₃-29% Bi₂Te₃-3% Sb₂Se; (●) n-type Bi₂Te₃-5% Sb₂Te₃; (□) p-type Bi₂Te₃; (■) n-type Bi₂Te₃; (△) p-type PbTe; (▲) n-type PbTe; (x) p-type AgSbTe₃. (From Ross, F. D., Solid State Electron., 11, 833, 1968. With permission.)

The maximum figure-of-merit in its dimensionless form ($Z_m T$) is then given by

$$Z_m T = \frac{4}{L_0} [\lambda_0/k_L] [1 + (\lambda_e/\lambda_L)] \quad (3)$$

Higher values of $Z_m T$ are obtained where $(\lambda_e/\lambda_L) \sim 0.5$. The variation of $Z_m T$ against (λ_0/k_L) for several thermoelectric semiconductors is displayed in Figure 1; the good agreement with the highly idealized theoretical formulation should be noted.

6.2 Requirement of Low Thermal Conductivity

"Good thermoelectric materials" obviously require a low thermal conductivity to prevent a significant portion of the heat from flowing down the temperature gradient. Most of the thermal conductivity studies that relate to thermoelectric materials have dealt primarily with the question of reducing the thermal conductivity without resulting in an adverse effect of the electrical power factor $\alpha^2\sigma$. However, there are considerable problems in achieving this objective. As the thermoelectric semiconductors are heavily doped, a significant contribution to thermal conductivity arises from the electrons (or holes). The nature of the problem is better realized when one considers the dependence of the figure-of-merit on two factors: the electrical properties of the material as incorporated in the power factor $\alpha^2\sigma$ and a degradation due to heat loss.¹⁴ The fact that a significant k_e is invariably present needs to be taken into account in any thermal conductivity minimization program.

Thermoelectric materials should possess a low value of thermal conductivity to reduce the loss of heat by conduction, and a reasonably large energy band gap to minimize the effect of the minority carriers.¹⁵ Usually the materials with large band gaps possess large lattice thermal conductivity. A plot of E_g vs. k_L for a number of commonly used semiconductors is displayed¹⁶

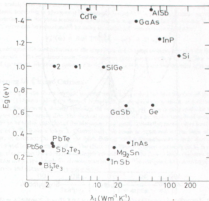


FIGURE 2 Lattice thermal conductivity and energy gap for various semiconductors. Si-Ge refers to 80-20 composition. (1) SiGe doped, 10^{19} m^{-3} ; (2) doped fine-grained. [From Bhandarkar, C. M. and Rose, D. M., Proc. Second Int. Conference Thermoelectric Energy Conversion, Arlington, 1978. With permission.]

in Figure 2. Any attempt to reduce λ_L without significantly affecting the band gap and the power factor $\alpha^2\sigma$ could lead to a better choice of thermoelectric material. For example, the effect of alloy disorder on λ_L in materials like Si-Ge alloys is significant (over a wide range of composition), whereas the band gap varies almost linearly when silicon is added to germanium.

6.3 Reducing the Lattice Thermal Conductivity

Alloy Disorder

A reduction in the lattice thermal conductivity can be achieved in several ways. The effect of introducing point-defects as in an alloy has been described in the context of Si-Ge alloys. The aim has primarily been to seek a selective scattering of phonons. Any mechanism that scatters phonons more effectively than the electrons (or holes) is likely to enhance the electrical to thermal conductivity ratio. Among the important scattering mechanisms that tend to reduce the phonon mean free path are scattering by other phonons, lattice defects, electrons and holes, and grain boundaries. One of the most thoroughly understood mechanisms related to defect scattering is based upon mass-difference scattering.^{2-5,17} The usefulness of solid solutions in thermoelectric applications was realized at an early stage and various recipes were put forward to improve the figure-of-merit by decreasing the thermal conductivity. The thermal conductivity of bismuth telluride-based solid solutions is displayed in Figure 3. Reductions of the phonon mean free path in solid solutions is analyzed in terms of mass-difference scattering with an associated phonon relaxation time.¹⁷

$$\tau_{pd}^{-1} = \Gamma \omega^2 g(\omega)/6N \quad (4)$$

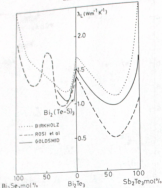


FIGURE 3. Lattice thermal conductivity of n-type Bi_2Te_3 alloys at 300 K. (From Goldsmid, H. J., in Materials Used in Semiconductor Devices, Hogarth, C. A., Ed., Interscience, 1965. With permission.)

Γ , which is a measure of the strength of the scattering, is given by

$$\Gamma = \frac{\epsilon}{M} \left(1 - \frac{M_i}{M} \right)^2 \quad (5)$$

ϵ is the fractional concentration of the impurity of mass M_i and $\bar{M} = \Sigma M_i$ is the mean atomic mass. For the Debye model $\text{g}(\omega) \propto \omega^2$ and the familiar Rayleigh expression is obtained

$$\tau_{pd}^{-1} = \Omega_d \Gamma u^4 / 4 \pi v_i^3 \quad (6)$$

$\Omega_d = V/N$ is the average atomic volume, v_i is the average sound (phonon) velocity, and u refers to the phonon frequency. Obviously this method of reducing λ_L is useful in alloys such as silicon-germanium where the atomic masses of the components differ considerably. In general an impurity atom differs from the host atoms in its mass, size, and the force constants. A generalized expression which takes these various factors into account can be written as^{21,22}

$$\Gamma_i = f_i [(\Delta M/M)^2 + 2[(\Delta G_i/G_i) - 6.4 \gamma (\Delta \delta_i/\delta_i)]^2] \quad (7)$$

G_i is the average stiffness constant of the nearest-neighbor bonds from the impurity to the host atom and G the corresponding quantity for the host. δ_i is the cube root of the atomic volume for the i th impurity in its own lattice and $\delta = \Sigma \delta_i$. γ represents the average anharmonicity of the bonds.

Resonance Scattering

Resonance scattering corresponds to a process in which phonons combine to excite a localized mode. Certain impurities in particular host lattices give rise to a scattering which results in small

dips or undulations in the thermal conductivity curves. The process may be understood in terms of inelastic scattering of phonons at the impurity modes.²³⁻²⁵ A resonance scattering relaxation time together with the usual scattering mechanisms is required to explain the results. The dip in the λ -T curve can be reproduced²⁶ by using an additional relaxation time given by²⁷

$$\tau_R^{-1}(n) = Rm^2 T^n / [(\omega_0^2 - \omega^2)^2 + D \omega^2 n^2] \quad (8)$$

R depends upon the concentration of the impurities and D refers to damping; ω_0 is the frequency characteristic of the resonance mode. For monatomic disturbances (such as KCl:NaCl) $n = 2$ gives a good agreement, whereas in systems like KCl:KNO₃, $n = 0$ is found to be more appropriate.

Scattering by Charge Carriers

Heavy doping of the thermoelectric material necessitates a detailed investigation of the role of carriers as (1) agents aiding the flow of heat down the temperature gradient, and (2) scattering centers for the phonons, thereby opposing the flow of heat. For some doping levels the two contributions may be comparable. The thermal conductivity of a particular sample of n-InSb is reported²⁷ to be higher than that of the corresponding undoped material; on the other hand a p-type sample of InSb shows a lower λ . Qualitatively this could be explained on the basis of a larger mobility of electrons than that of the holes. A large mobility may lead to a large electrical conductivity and hence an enhanced λ_e . The effect of additional phonon scattering on λ_e is obviously less significant than the additional electronic contribution to the flow of heat. The same could not be said for the p-type sample for obvious reasons. Ziman^{28,29} investigated the scattering of phonons by carriers and obtained the relaxation time

$$\tau_{pe}^{-1} = \frac{e^2 m^{*2} k T}{2 \pi \hbar^2 p v_L} \left[z - \ln \left[\frac{1 + \exp(\phi + z/2)}{1 + \exp(\phi - z/2)} \right] \right] \quad (9)$$

where $z = \hbar \omega / k T$ and

$$\phi = \hbar^2 \omega^2 / 8 m^{*} v_L^2 k T + m^{*} v_L^2 / 2 k T - E_F / k T \quad (10)$$

Here e is the strength of the electron-phonon interaction and E_F is the Fermi energy. v_L refers to the average phonon velocity and the various other parameters have their usual meanings. This expression has been derived for the longitudinal phonons. The expression can be simplified with the inverse relaxation rate expressed¹³ in terms of z , i.e., $\tau_{pe}^{-1} = B' z$, where the proportionality constant B' represents the strength of phonon-electron scattering.

The role of the carriers as scattering centers along with that of heat carriers is displayed³⁰ in Figure 4 in which the thermal conductivity of n-Bi₂Te₃ is plotted against electrical conductivity. The region of the minimum is of obvious interest in thermoelectric applications. A theoretical analysis³¹ of the results must take into account the effects of the multivalley band structure, non-parabolicity of bands and that of the minority carriers. The bipolar contribution to thermal conductivity is significant in the region beyond the minimum.

Scattering by Grain Boundaries

The phonon mean free path may be limited by crystal dimensions. A mean free path (l_b) can be defined which is related to the crystal size; $l_b = 1.12 D$, for a specimen with square cross section of side D. Berman and coworkers³² have presented a detailed theory of boundary scattering which takes into account different surface conditions.

Earlier accounts of boundary scattering portrayed it as a low-temperature phenomenon. However, in highly disordered materials, boundary scattering may become significant at high temperatures.³³ A high degree of disorder effectively scatters short-wavelength phonons with the net heat conduction being primarily due to long-wavelength phonons. These may then be scattered effectively by the grain boundaries and result in significant reduction in thermal conductivity. Experiments on thin specimens of silicon showed a pronounced decrease in the thermal conductivity due to boundary scattering which was enhanced in samples irradiated with neutrons.^{34,35}

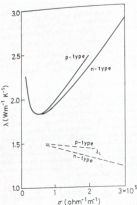


FIGURE 4 Thermal and electrical conductivities of n-type Bi₂Te₃ at 300 K. (Goldsmid, H. J., Proc. Phys. Soc., 72, 17, 1958. With permission.)

Parrott¹⁶ further explored the consequences of grain boundary scattering in fine-grained materials. Considering the high temperature limit (hbarT < 1, ω referring to average phonon frequency), it is possible to obtain compact simplified formulae for the thermal conductivity which take into account phonon scattering by phonons, grain boundaries, disorder, and electrons. The phonon relaxation times for the Umklapp process is given by

$$\tau_U^{-1} = A_U z^2 (z = \hbar\omega/kT) \quad (11)$$

The Normal process relaxation time is assumed to have the same frequency dependence with $\tau_0 = k_0 \tau_0$, where k_0 is an adjustable parameter. The thermal conductivity can be conveniently expressed¹⁶⁻¹⁸ in terms of the conductivity of the virtual perfect crystal (λ_0), in which phonon-phonon scattering is the only mechanism which limits the phonon mean free path. The remainder of the expression accounts for all other phonon scattering processes. The thermal conductivity is given by

$$\lambda/\lambda_0 = (1 + 5k_0/9)^{-1} \left[L_2 + \frac{k_0(1 + k_0)^{-1} L_4^2}{0.2 - k_0(1 + k_0)^{-1} L_4} \right] \quad (12)$$

where

$$L_n = \int_0^1 \frac{x^n dx}{Ax^2 + x^2 + Bx + C} \quad (13)$$

The parameters representing the strengths of the scattering by alloy disorder, free carriers, and grain boundaries are given by

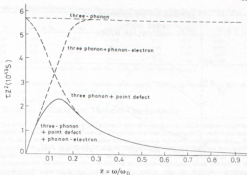


FIGURE 5 Integrand in the thermal conductivity expression plotted against reduced phonon frequency ω/ω_0 for various phonon scattering processes. [From Steigmeier, E. F. and Abelson, B., Phys. Rev. A, 136, 1149, 1964. With permission.]

$$A = \frac{\pi \lambda_0 \Gamma k_{\text{B}} \omega_0}{2\pi^2 k (1 + 5k_0/9)} \quad (14)$$

$$B = \frac{2\pi^2 k_0 \nu AB'}{\omega_0^2 k^2 T (1 + 5k_0/9)} \quad (15)$$

$$C = 2\pi^2 k_0 \nu^2 / L k \omega_0^3 (1 + 5k_0/9) \quad (16)$$

With the help of these equations it is possible to explore the effects of the different scattering processes which operate in relevant thermoelectric materials. The factor $(1 + 5k_0/9)$ takes into account (in an approximate way) the special role of the N-processes. The parameters A, B, C represent the strength of scattering by alloy disorder, electron-phonon, and grain boundaries. To appreciate the relative roles and strengths of these phonon scattering mechanisms it is instructive to plot²⁹ the integrand of the thermal conductivity integral against the reduced phonon frequency x (Figure 5). In a pure (unalloyed) undoped, single crystal ($A = B = C = 0$) the integrand is almost independent of x . The effect of alloying ($A > 0$) is to reduce the integrand considerably in the high-frequency region. The high-frequency phonons having been effectively scattered, most of the heat is carried by low-frequency phonons. The boundary scattering can then effectively scatter low-frequency phonons. It is easy to appreciate the increased effectiveness of boundary scattering in the presence of alloy disorder. Bhandari and Rowe¹⁸ have also discussed the effect of dispersive phonon branches on the lattice thermal conductivity.

6.4 Fine-Grained Materials

Improving the Ratio of Electrical to Thermal Conductivity

An understanding of the relative roles of the various mechanisms in limiting the phonon mean free path may find application in thermoelectric material development. The preparation of fine-grained materials of the required grain size and with the required degree of disorder can effectively

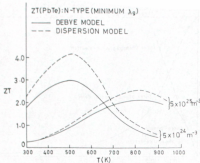


FIGURE 6. ZT plotted against temperature for the Debye and dispersive models. (From Goff, G. F. and Lowrey, J. R., Proc. 10th IBEC, 1958, p. 1961. With permission.)

reduce the thermal conductivity. Implicit in these considerations is the realization that the electrical conductivity is not significantly influenced by the grain boundaries. Various studies have suggested appreciable improvement in the figure-of-merit of fine-grained silicon-germanium alloys.³⁰⁻³² The study was extended^{33,34} to lead telluride-based alloys; a grain size of 1 μm could reduce the lattice thermal conductivity of these alloys by around 11 to 13%. Several review papers^{31,34-36} present details of the state of the art.

Slack and Hussain³⁷ have discussed the changes in the electrical and thermal conductivities of Si-Ge alloys that accompany boundary scattering and their results are not in agreement with the earlier reported improvements in the electrical to thermal conductivity ratio. Sample preparation and history are important and need to be taken into consideration before conclusions can be drawn about the degree of effectiveness of grain boundary scattering in improving thermoelectric materials.

Other Considerations

Most of the efforts towards reducing the thermal conductivity described so far have been related to limiting the phonon mean free path l . The simple equation for the thermal conductivity expresses it in terms of the lattice specific heat, sound (phonon) velocity, and l . The simple Debye model is usually used for describing phonon modes, and does not distinguish between various polarizations, and assumes a constant phonon velocity $v_p = v$. However, this is not always justifiable and the phonon branches may exhibit strong dispersion which has a profound effect on phonon transport. Among the better-known thermoelectric semiconductors, silicon-germanium and lead telluride have strongly dispersed phonon branches. At high frequencies the group velocity becomes very small and in some cases even negative. This may have two consequences: k_L may be lower than that obtained on the basis of the Debye model, and the alloy disorder may become less effective as the high-frequency phonon contribution has been reduced due to the dispersive effects.

Goff and Lowrey³¹ obtained the lower bound of k_L in PbTe by assuming $(\lambda_L)_{\text{min}} = \text{lattice spacing}$. This gives the high-temperature values of λ_{min} as 0.126 W/mK and 0.06 W/mK for the Debye and dispersive models, respectively. A plot³¹ of ZT vs. T obtained with these λ_L values is shown in Figure 6. It is interesting to note that ZT now has a higher value for lower carrier concentrations,

Table 1. Calculated Values of Various Thermoelectric Parameters for n-Type Si_{0.9}Ge_{0.1} Alloy at 300 K.

<i>f</i>	<i>n</i> (10 ¹⁹ m ⁻³)	<i>-αθ</i> (μV/K)	<i>σ</i> (10 ³ Ω ⁻¹ m ⁻¹)	<i>k_a</i> (10 ⁻³)	<i>k_L</i> (W/mK)	<i>Z</i> (10 ⁻⁴ K ⁻¹)
0.0	1.25	136.5	1396.6	8.73	42.73	0.432
0.3	0.65	384.2	862.3	4.85	21.51	0.852
0.6	0.45	213.0	473.5	3.46	13.59	1.256
1.0	0.35	233.5	374.6	2.74	9.00	1.740

[From Slack, G.A. and Hussain, M., *J. Appl. Phys.* 70 (9), 2894, 1991. With permission.]

whereas for normal λ_L values the situation was the reverse. These considerations might have implications in future material research programs.

6.5 Towards a Minimum Thermal Conductivity

The efforts to reduce λ_L are likely to continue in spite of a significant λ_a , which seems to be ignored in theoretical formulations. The concept of a minimum of thermal conductivity was first discussed by Roufosse and Klemens.⁴⁹ Slack⁴⁷ elaborated the theoretical framework and calculated λ_{\min} for a number of crystals. In general both acoustic and optical phonons contribute and their contributions to λ_{\min} have been obtained by Slack. The theoretically obtained values of λ_{\min} are then compared with the observed values which refer to the high-temperature values obtained by extrapolating the observed thermal conductivity to the melting point. The results for a number of crystals with two atoms per unit cell have been reported.⁴⁷ It is to be noted that the observed thermal conductivity at the melting point for some rocksalt structure materials is higher than the calculated minimum by a factor of 2. For adamantine crystals this may increase to 7. This serves to indicate that even at the melting point the lowest thermal conductivity has not been reached and that there is scope for further reduction.

Understandably the minimum refers to a value of thermal conductivity when the phonon mean free path is close to the phonon wavelength. This is essentially similar to the amorphous case and therefore data on amorphous samples can provide an estimate of λ_{\min} . For Si_{0.9}Ge_{0.1} Slack and Hussain used $\lambda_{\min} = 0.9$ W/mK in their calculations. In general any sample may have its λ_L between two limits:

$$\lambda_G \geq \lambda_L \geq \lambda_{\min} \quad (17)$$

where λ_G is the thermal conductivity value in pure samples determined from the observed values. It could be obtained as a $T^{-1/2}$ variation^{28,30} for temperatures above room temperature. Slack and Hussain express thermal conductivity in resistivity terms and define a parameter *f* where

$$1/\lambda_L = (1 - f)/\lambda_G + f/\lambda_{\min} \quad (18)$$

The parameter *f* represents the fraction of the progress made towards achieving λ_{\min} . Table 1 presents the results of their calculations for silicon germanium at 300 K. A calculation like this is useful in the context of thermoelectric material research. However, for a quantitative estimate of the electronic transport coefficients the effect of band non-parabolicity⁵⁰⁻⁵² must be taken into consideration, particularly at the high doping levels required for thermoelectric applications.

References

1. Ziman, J. M., *Electrons and Phonons*, Cambridge University Press, London, 1960.
2. Drabble, J. R. and Goldsmith, H. J., *Thermal Conduction in Semiconductors*, Pergamon Press, London, 1961.
3. Parratt, J. E. and Stuckes, A. D., *Thermal Conductivity of Solids*, Pion Limited, London, 1975.
4. Berman, R., *Thermal Conduction in Solids*, Clarendon Press, Oxford, 1976.
5. Bhambhani, C. M. and Rose, D. M., *Thermal Conduction in Semiconductors*, Wiley Eastern Limited New Delhi, 1988.

6. Joffe, A. F., *Semiconductor Thermoelements and Thermoelectric Cooling*, Insituress, London, 1957.
7. Cadoff, E. B. and Miller, E., Eds., *Thermoelectric Materials and Devices*, Reinhold, New York, 1959.
8. Goldsmid, H. J., *Applications in Thermoelectricity*, Methuen Monograph, London, 1960.
9. Uso, R. W. and Heikes, R. R., Eds., *Thermoelectricity: Science and Engineering*, Interscience, London, 1961.
10. Rose, D. M. and Bhandari, C. M., *Modern Thermoelectricity*, Holt Saunders, London, 1983.
11. Rashba, Y. I., Efimov, B. A., and Steyrnko, I. A., in *Semiconducting Lead Chalcogenides*, Sti'Bans, T. S., Ed., Pleum, New York, 1976.
12. Ravich, Y. I., Efimov, B. A., and Tsvartchenko, Scattering of current carriers and transport phenomena in lead chalcogenides (II), *Phys. Status Solidi (b)*, 43, 11, 1971.
13. Chamaa, R. P. and Statton, R. J., The thermoelectric figure of merit and its relation to thermoelectric generation, *J. Electron. Control.*, 7, 52, 1958.
14. Goff, G. F. and Lowney, J. R., The integral formulation for the thermoelectric figure-of-merit effects of a lattice thermal conductivity, *Proceedings of 11th ITC-E*, 1976, p. 1561.
15. Bhandari, C. M. and Rose, D. M., Minority carrier effects of the thermoelectric figure-of-merit, *Proceedings of 1st European Conference on Thermoelectricity*, 1988, p. 178.
16. Rose, D. M. and Bhandari, C. M., Fine-grained Si-Ge alloys as superior thermoelectric materials, *Proceedings of 2nd International Conference on Thermoelectric Energy Conversion*, University of Texas at Arlington, 1978, p. 31.
17. Klemens, P. G., The scattering of low frequency lattice waves by lattice imperfections, *Proc. Phys. Soc. (London) A*, 68, 1113, 1955.
18. Goldsmid, H. J., in *Materials Used in Semiconductor Devices*, Hogarth, C. A., Ed., John Wiley, Interscience, London, 1965, 163.
19. Birkholz, U., Z. Naturforsch., 13a, 768, 1958.
20. Ross, F. D., Abeyes, B., and Jensen, R. V., *J. Phys. Chem. Solids*, 10, 191, 1959.
21. Carruthers, T., *Rev. Mod. Phys.*, 33, 92, 1961.
22. Abeyes, B., Lattice thermal conductivity of dispersed semiconductor alloys at high temperatures, *Phys. Rev.*, 131, 1806, 1963.
23. Holland, M. G. and Snareyler, L. J., *Proceedings of the International Conference on Physics of Semiconductors*, Ernest, The Institute of Physics and Physical Society, London, 1962, p. 35.
24. Vook, F. L., Thermal conduction of electron-irradiated silicon, *Phys. Rev. A*, 146, 2013, 1965.
25. Wagner, M., Influence of localized modes on thermal conductivity, *Phys. Rev.*, 131, 1443, 1963.
26. Walker, C. T. and Pohl, R. O., Phonon scattering by point defects, *Phys. Rev.*, 131, 1433, 1963.
27. Stacker, A. D., Thermal conductivity of indium antimonide, *Phys. Rev.*, 107, 427, 1957.
28. Ziman, J. M., The effect of free carriers on lattice conduction, *Philos. Mag.*, 1, 191, 1956.
29. Ziman, J. M., The effect of free carriers on lattice conduction, *Philos. Mag.*, 2, 282, 1957.
30. Goldsmid, H. J., *Proc. Phys. Soc.*, 72, 17, 1958.
31. Bhandari, C. M. and Agrawal, V. K., Thermal and electrical transport in biomath telluride, *Indian J. Pure Appl. Phys.*, 28, 448, 1990.
32. Bernstein, R., Foster, E. L., and Zisman, J. M., Thermal conduction in artificial sapphire crystals at low temperatures, *Proc. R. Soc. A*, 231, 130, 1955.
33. Goldsmid, H. J. and Penn, A. W., Boundary scattering of phonons in solid solutions, *Phys. Lett. A*, 27, 523, 1968.
34. Savvides, N. and Goldsmid, H. J., The effect of boundary on the high temperature thermal conductivity of silicon, *J. Phys. C: Solid State Phys.*, 6, 1701, 1973.
35. Savvides, N. and Goldsmid, H. J., *Phys. Status Solidi (b)*, 63, K89, 1974.
36. Parrott, J. E., The thermal conductivity of sintered semiconductor alloys, *J. Phys. Chem.*, 2, 147, 1968.
37. Meddler, H. R. and Parrott, J. E., The thermal and thermoelectric properties of sintered Ge-Si alloys, *J. Phys. C: Solid State Phys.*, 9, 1263, 1976.
38. Bhandari, C. M. and Rose, D. M., Boundary scattering of phonons, *J. Phys. C: Solid State Phys.*, 11, 1787, 1978.
39. Strigemeier, E. F. and Abeyes, B., *Phys. Rev.*, 136, 1149, 1964.
40. Rose, D. M. and Bhandari, C. M., Effect of grain size on the conversion efficiency of semiconductor alloys at high temperatures, *Appl. Energ.*, 6, 347, 1980.

41. Bhandari, C. M. and Rose, D. M., Silicon-germanium alloys as high temperature thermoelectric materials, *Congr. Phys.*, 21, 219, 1980.
42. Bhandari, C. M. and Rose, D. M., The effect of phonon grain boundary scattering, doping and alloying on the lattice thermal conductivity of lead telluride, *J. Phys. D: Appl. Phys.*, 16, L75, 1983.
43. Rose, D. M. and Bhandari, C. M., Lattice thermal conductivity of small grain size PbSnTe and PbGeTe thermoelectric materials, *Appl. Phys. Lett.*, 47, 256, 1985.
44. Rose, D. M. and Bhandari, C. M., Preparation and thermal conductivity of doped semiconductors, *Prog. Cryst. Growth Charact.*, 13, 233, 1986.
45. Rose, D. M. and Bhandari, C. M., A review of lead telluride technology at UWIST, *Sixth Int. Conf. on Thermoelectric Energy Conversion*, Arlington, 1986, p. 43.
46. Parrott, J. E., Thermal conductivity: a guide to improved thermoelectric materials, *Proceedings of the Int. European Conference on Thermoelectrics*, Cardiff, 1988, p. 187.
47. Slack, G. A. and Hussain, M., The maximum possible conversion efficiency of Si-Ge thermoelectric generators, *J. Appl. Phys.*, 70(5), 2694, 1991.
48. Routledge, M. and Klemens, P. G., *J. Graphyn. Res.*, 79, 703, 1974.
49. Slack, G. A., The thermal conductivity of nonmetallic crystals, in *Solid State Physics*, Turnbull, D. and Eshenroder, H., Eds., Academic Press, New York, 1979, 34.
50. Abeles, B., Beers, D. S., Cody, G. D., and Darnakes, J. P., Thermal conductivity of Ge-Si alloys at high temperature, *Phys. Rev.*, 125, 44, 1962.

17

Z-Meters

Hugh H. Woodbury,
Lionel M. Levinson, and
Robert S. Lewandowski
General Electric Company
Schenectady, New York, U.S.A.

17.1 Introduction	181
17.2 A Large Temperature Difference Z-Meter	182
Design Features • Operation and Calibration • Analysis of Data	182
17.3 Design Considerations: Problems, Promises, and Solutions	185
17.4 Summary and Recommendations	187
References	187

17.1 Introduction

The thermoelectric figure-of-merit, Z , is defined as:

$$Z = \alpha^2 / (\lambda p)$$

where α is the Seebeck coefficient, λ the thermal conductivity, and p the electrical resistivity.¹ Z is a common measure of the effectiveness of a material to function in a thermoelectric couple for heating or cooling applications. A knowledge of the temperature dependence of Z is important in optimizing couples for specific applications.

A Z-meter is an instrument that simultaneously measures, on one sample, the three thermoelectric parameters of interest as a function of temperature from which Z can be calculated. Putley² describes an apparatus which he used to measure the Peltier heating and cooling when a small current was passed through a sample. The resulting small temperature difference gives rise to a Seebeck voltage, and the thermal conductivity can be calculated from the steady-state conditions. Independently, Harman et al. used the same idea in a Z-meter.³ An interesting feature of this approach is that ZT , where T is the absolute temperature, can be directly determined from the experimental data as a ratio of the various measured voltages. Linker briefly outlines a general analysis of this approach, pointing out that a variety of different but related measurements which lead to Z or ZT can be carried out.⁴ A number of experimental variations of these ideas have been proposed, including the study of films. Accurate measurement of α , λ , and p requires care. In particular, measurement of the thermal conductivity is difficult and needs a steady-state condition and adiabatic thermal insulation of the sample or appropriate corrections for the lack thereof.⁵

The primary interest of the above cited authors was the study of materials for thermoelectric cooling, i.e., making measurements near or below room temperature, although Putley's apparatus employed a sample holder that could be heated to 700°C,² while Phillips⁶ and Kaplan⁷ have described Z-meters that operate in the range 100 to 600°C. They essentially involve a classical arrangement for directly measuring α , λ , and p on rod-shaped samples. The need for establishing different thermal conditions for each measurement, i.e., a moderate temperature gradient for α , a low gradient for λ , and a zero gradient for p , illustrates a major difficulty in these approaches. Automated versions of this classical stationary approach have been described by Wartanowicz and Goszczoński⁸ and by Vedernikov et al.⁹

An alternative approach to Z-meters employs a large temperature difference across the sample.^{10–12} The total Seebeck voltage, thermal conductance, and electrical resistance are essentially simultaneously measured as a function of the temperatures of the ends of the sample. The data are then deconvoluted to obtain the temperature dependence of α , λ , and p , from which the temperature dependence of Z is determined. A computer is used to record the data, and the method

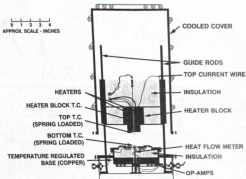


Figure 1 Overall schematic of the large temperature difference apparatus, which is shown here without a sample and with the cover slightly lifted. Not shown are the supports for the top thermocouple and the top bracing to carry the added weights to increase the contact pressure on the ends of the sample.

results in a fully automated system for a complete temperature run. This is one of its principal advantages. A description of such a meter is given in Section 17.2. This description provides a context for discussion of more general Z-meter problems, which are considered in Section 17.3.

Section 17.4 gives a summary and recommendations for the use of Z-meters. The promises of Z-meters are many, including the automated, reproducible measurement of the basic thermoelectric parameters and not relying on data taken on different samples or in sequence on the same sample. For example, the trade-off between the Seebeck coefficient and electrical resistivity for semiconductors is well known, and typical sample-to-sample variations or variations following thermal cycling in which the active dopant concentrations change can give misleading results if measurements are carried out in sequence or on different samples.

17.2 A Large Temperature Difference Z-Meter

Design Features

In this section we give the detailed design specifications, operation and calibration features, and data analysis for a particular large temperature difference Z-meter. This meter has been used successfully by the authors to up to 700°C for samples 6.3 mm square by 1 to 1.5 cm long. While this meter was constructed to measure specific thermoelectric materials having properties similar to those of PbTe alloys, the authors believe this type of meter has a broader usefulness and the details given here relate to general Z-meter design considerations.

The features of the Z-meter are shown in Figures 1 and 2. Construction details are as follows: the top and bottom supports for the heater block are quartz disks secured to the stainless steel cylinder with screws "padded" with high-temperature silicone rubber. This upper assembly is guided with Teflon^{*} bearings on stainless steel rods. The insulation is quartz wool throughout. An

^{*}Teflon is a registered trademark of E.I. du Pont de Nemours and Company Inc., Wilmington, DE.

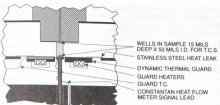


FIGURE 2 Details of the sample area and heat flow meter of the large temperature difference apparatus. Not shown are the sample end gaskets and the insulation (quartz wool) which surrounds the sample.

additional 1-kg weight is placed on top of the stainless steel cylinder to counter the force of the spring-loaded upper and lower thermocouples and to increase the contact pressure on the sample ends.

In order to preserve the face of the bottom of the heater block, a thin sheet of Pt is brazed onto it and is then machined and polished. A 5-mil Grafel^{*} gasket is used at the top while two 2-mil indium gaskets are used at the bottom to provide uniform electrical and thermal contacting. The bottom of the sample never gets above 120°C. The apparatus is evacuated and back-filled with argon before a measurement run.

One objective of the design is to create a vertical heat flow pattern adjacent to the sample by creating uniform temperature planes at the top and bottom of the sample. The bottom of the heater block forms the top plane while a dynamic thermal guard ring around the top of the heat flow meter forms the bottom plane. This guard ring is maintained close to the temperature of the bottom of the sample by comparing the reading of the guard thermocouple with the heat flow meter output signal. The difference signal is used to control the guard heaters in a standard analog control loop.

The dynamic thermal guarding of the heat flow meter and the use of cooling coils around the outside shield improve the reproducibility from run to run and significantly decrease the time required to bring the system into thermal equilibrium before a run begins.

Molybdenum was the choice for the heater block because of its higher thermal conductivity over high-temperature alloys such as Inconel. This provides a higher maximum temperature at the top of the sample for a given (maximum) temperature rating of the heaters as well as maintaining a more uniform temperature plane.

Some electrical considerations are as follows: the heat flow meter is made of copper to give rapid thermal response. A 5-mil constantan wire is secured to the top of the square copper pedestal comprising the meter. This wire and the copper meter and base become a thermocouple pair which generates the meter output signal. The upper thermocouple is a 5-mil platinum-platinum/10% rhodium pair in a 47-mil O.D. zirconia tubing. The lower thermocouple is a copper-constantan pair in similar zirconia tubing. Both of these thermocouples are referenced to the base, which is maintained at 25°C with a VWR Model 1145 Constant Temperature Circulator (VWR Scientific Inc., San Francisco, CA).

The leg-pairs of the thermocouples are each brought to the inputs of AD708 operational amplifiers (Analog Devices, Inc., Norwood, MA) connected in an instrumentation mode. The time constant is designed to be 100 msec and the measured input noise is <0.5 µV. In order to measure the Seebeck voltage, the Pt and Cu legs of the upper and lower thermocouples are carried to a fourth AD708, also with a time constant of 100 msec. All of the op-amps are mounted such that

*Grafel is a registered trademark of Union Carbide Corp., New York, NY.

they are in thermal contact with the base, which provides excellent stability. Occasionally the system is permitted to equilibrate for 24 to 48 h, at which time the zero offset readings are read and stored by the computer.

To measure the resistivity, a square wave current pulse is passed through the sample. This pulse is computer-controlled in timing and duration as well as magnitude. Typically it is 60 msec positive and 60 msec negative and ± 1 A in magnitude. The ohmic voltage drop across the sample is measured through the same thermocouple legs used for measuring the Seebeck voltage. However, they feed a parallel AD708 with a time constant of 4.7 msec. The faster response time of this circuit minimizes distortion of this pulse.

The outputs from the five op-amps plus a current signal derived from the voltage drop across a 1- Ω standard resistor are fed into a DT2801/5716A 16-bit A/D board (Data Translation, Inc., Marlboro, MA) plugged into a PC. Care is taken to balance the impedances of all lines to maintain a high CMRR.

Operation and Calibration

The end faces of the samples are ground using simple jigs to ensure that they are planar and parallel. Accurately centered and defined thermocouple wells (see Figure 2) are made using a clockmaker's precision drill press with 50-mil diamond drills (Diamond Microdrill #550, Amplex Corp., Bloomfield, CT).

To begin a measurement run, data near room temperature, typically from 25 to 50°C, are first obtained by applying low power to the heater block. Also, the voltage waveform at the output of the current square wave generator is monitored with a digital scope. This initial testing provides (1) a check on the sample integrity, (2) a check on the electrical and thermal contacting, (3) a check to optimize the software-controlled A/D channel gains and the magnitude of the current pulse (for new samples with unknown characteristics), and (4) approximate, near room temperature values for the thermoelectric parameters before the sample is thermally cycled. The initial near room temperature measurements check for any sample hysteresis.

Following the initial checks, full power of 200 W is applied to the heater block, which brings it to 500–600°C in about 30 min. After a holding period of 30 min, the heater block power is turned off and the whole assembly is allowed to cool. The upper thermocouple is continuously monitored by the computer, and at preset intervals (typically 10°C), data collection is initiated. Each data collection cycle consists of reading the upper and lower thermocouples, the heat flow meter, and the Seebeck voltage. The current pulse is then generated, and the current and sample ohmic voltages are measured. A complete set of data is taken in 150 msec. The last data point is usually taken at 30°C, 5°C above the base. The entire temperature range is covered in 6 to 12 h. Since the data collection is under computer control, run-to-run reproducibility is very good.

The temperature measurements are better than 0.1°C on a relative basis. The absolute temperature values are no better than typical thermometry accuracy but are not critical in the analysis.

Analysis of Data

To convert the Seebeck voltages, electrical resistances, and the sample thermal conductances to the Seebeck coefficient, resistivity, and thermal conductivity as a function of temperature, it is necessary to deconvolute the experimental data. This is done using the following relationships:

$$\text{Measured Seebeck voltage} = V_s = \int_{T_i}^{T_b} \alpha \cdot dT \quad (1)$$

$$\frac{\partial V_s}{\partial T_b} = \alpha(T_b) - \alpha(T_i) \frac{\partial T_c}{\partial T_b} \quad (2)$$

$$\text{Measured heat flow} = Q = (A/L) \int_{T_i}^{T_b} \lambda \cdot dT \quad (3)$$

$$(L/A) \cdot \frac{\partial Q}{\partial T_h} = \lambda(T_h) - \lambda(T_c) \frac{\partial T_c}{\partial T_h} \quad (4)$$

$$\text{Measured resistance} = R = (1/Q) \int_{T_c}^{T_h} \rho \cdot \lambda \cdot dT \quad (5)$$

$$\frac{\partial(R \cdot Q)}{\partial T_h} = \rho(T_h) \cdot \lambda(T_h) - \rho(T_c) \cdot \lambda(T_c) \cdot \frac{\partial T_c}{\partial T_h} \quad (6)$$

where A is the cross-sectional area and L the length of the sample minus the depths of the thermocouple wells. The essence of the formulation of Equations 1, 3, and 5 is that the integrals are independent of the actual temperature gradient in the sample and hence are functions only of T_h and T_c .

$\Omega(T_h)$, $\lambda(T_h)$, and $\rho(T_h) \cdot \lambda(T_h)$ are solved iteratively using equations 2, 4, and 6. Note that when most of the temperature drop is across the sample ($\partial T_c / \partial T_h \ll 1$). Also, $\Omega(T_h)$, $\lambda(T_h)$, and $\rho(T_h)$ do not change rapidly with T_h . Thus, $\Omega(T_h)$, $\lambda(T_h)$, and $\rho(T_h)$ can be determined quickly and accurately in a simple iterative computer program. The partial derivatives are calculated using a finite difference method to determine the slopes of the desired quantities as a function of T_h . Three- and five-point slope calculations have been used.

17.3 Design Considerations: Problems, Promises, and Solutions

A Z-meter is inherently an instrument whose design requires compromises. As one example, proper electrical resistivity measurements require a uniform sample temperature while thermal conductivity and Seebeck coefficient measurements require a (small) temperature gradient. Furthermore, a four-point probing technique is required for λ and ρ measurements to minimize end contact effects, but standard-type side probes will disturb the axial heat flow. The arrangement shown in Figures 1 and 2 appears to be a suitable compromise.

While the Seebeck coefficient measurement is the simplest because it is independent of sample geometry, it does require corrections because of the thermoelectric power of the probe leads¹³ and also accurate temperature measurements. An attractive feature of the design is that both the top and bottom thermocouples are thermally guarded, the top by the essentially uniform temperature of the heater block and the bottom by the low temperature gradient in the heat flow meter. The use of zirconia sleeving instead of silica reduces the heat transport by the sleeving.

Although the total resistance of the sample is little changed by the wells, the distortion of the equipotential lines under the wells, which is basically a function of the radius of the wells, is significant. Computer modeling for 50-mil diameter wells in a 6.3-mm square cross section sample indicates that an effective length can be used to correct for the wells when calculating the resistivity. Specifically, $L(\text{eff}) = (L - 0.095)$ cm where L is the length between well bottoms. For 1- to 1.5-cm long samples, this correction is essentially independent of well depths up to the 35 mil which were modeled. The potential along the bottom of the wells varies little near the center, which means that the size of the thermocouple bead and its location in the well are not critical.

The effect of the wells on the thermal conductivity are not important because (1) the wells are not a thermal void because of the presence of the thermocouple wires/sleeving and argon and (2) the heat flow meter is usually calibrated with a reference sample having an identical geometry to the test samples. However, an absolute calibration of the heat flow meter was made using the known properties of copper. Up to 300°C, the results agree within 2% with a Pyroceram 9606 reference sample.¹⁴ This degree of agreement is fortuitous (although the temperature dependence is not) because the accuracy of the calculation is limited by the ability to model the foot and shoulder of the heat flow meter.

Typically 80% of the temperature drop is across the sample and 20% across the heat flow meter. The large temperature drop in the sample means that the final values obtained for any one parameter at a given temperature are not spatially averaged over the sample. Specifically, since the

temperature of the hot end is changing most rapidly, it contributes the bulk of the signal during a run. Also, because of the temperature dependence of the various parameters, the weighted contribution of each part of the sample changes with temperature. To check the assumption of sample uniformity, runs can be repeated with the sample turned over.

A final anomalous situation is that a thermal steady-state condition never exists in this instrument. Usually, under such conditions, corrections for the heat capacity of the sample have to be made. However, as long as the thermal mass of the heater block is much larger ($>100\text{C}$) than the thermal mass of the sample, this correction can be neglected. Under such conditions, taking data as the instrument naturally cools, the heat flowing through the sample from the heater block is always large compared to the internal heat of the sample. The cooling rates at 600°C , for example, are of the order of $10^\circ\text{C}/\text{min}$ while it may take 1 or 2 h to cool from 40 to 30°C . These are the proper rates and cannot be speeded up without making heat capacity corrections. It is important in the deconvolution to obtain data near the base temperature, although this takes the bulk of the time. In practice, one simply lets the meter collect data overnight.

The above assumes that the major heat loss of the heater block is entirely through the sample. Good insulation around the heater block is thus important in order to minimize the size of the heater block, i.e., its total thermal mass.

Insulation around the sample is also critical. The assumption of only axial heat flow, i.e., no radial flow into or out of the sample, is only approximated because, for most materials, the thermal conductivity changes significantly with temperature. This results in a nonuniform temperature gradient in the sample; however, the apparatus was designed to create a uniform gradient outside the sample. The mismatch between these gradients will produce a radial heat flow, which is believed to be the largest source of error for the heat conductivity and electrical resistivity values above 500°C .

Close-fitting, ideal thermal insulation around the sample would resolve this problem (as it would resolve many problems in thermal measurements). Looking to the future, high-temperature aerogels might approximate such a material.

At present, several approaches to the radial heat flow/insulation problem can be considered. One is to design for samples with large cross-sectional areas. Also, calibration should be done with reference samples which have a similar temperature dependence of the thermal conductivity. This is just as important as choosing a reference sample with similar average values. In any case, the relative comparison of samples of the same material is still valid even if the absolute values are in error.

The use of vacuum would greatly improve the thermal insulation. However, the thermal contacting to the ends of the sample and of the thermocouples with the sample would be severely degraded.

A final solution to the nonuniform temperature gradient across the sample is to design a "low temperature gradient" meter, i.e., one in which the temperature drop across the sample is 20% or less of the total. The general principles and analysis involved are the same as described above. The design problems, however, shift to the heat flow meter where the response time of the heat flow meter and thermal guarding of the lower thermocouple would be two of many considerations.¹⁵

A high signal-to-noise ratio is important because changes in the slopes of the measured data as a function of temperature, i.e., point-by-point differences, determine the final temperature dependence of the desired parameters. An alternative procedure is to fit the raw data to analytical functions, thereby smoothing the data, and then taking the derivatives of the functions. The functions cannot be too complicated or they will reflect the noise rather than average the data. However, our experience is that simple functions cannot fit the data over the full temperature range. Fitting fourth-degree polynomials over 100 to 200°C intervals and matching the parameters at the interval edges have proven successful.

By thermally isolating the base and using a refrigerant in the base cooling coils, the meter could be used to study materials for cooling applications down to -40°C . Since a much more limited temperature range is usually of concern for such materials, many of the problems mentioned above are reduced. Also, with the preamps thermally tied to the lower temperature, a reduction in amplifier noise would be realized.

Anisotropic materials, e.g., bismuth telluride,¹⁸ with grain sizes a significant fraction or larger than the size of the wells present formidable problems. The only satisfactory procedure we have found using our meter is to first measure the resistivity at room temperature on a large area sample or test puck using soldered contacts. This test puck is then cut into several smaller samples to fit the Z-meter where standard runs are carried out. The temperature-dependent resistivity values obtained are then normalized to the original room temperature values obtained on the original piece. Since spatial nonuniformities are often found in large test packs, e.g., from the center to the edges, more than one sample measurement in the Z-meter is often required per test puck.

Alternatively, samples could be prepared for the Z-meter without wells but with soldered metal end pieces. An emphasis in our design is to make sample preparation as simple as possible. Wells are included to get "four point probe" contacting to eliminate contact impedance when using pressure contacts and gasketing material. For high-temperature studies, this appears to be the simplest procedure because high-temperature brazing would otherwise be required, and there could be problems of chemical reactions or welding to the bottom of the heater block. However, for low-temperature anisotropic materials, metal end contacts appear to offer significant advantages.

17.4 Summary and Recommendations

The inherent advantages of an automated Z-meter are such that the inability to create a universal meter for any type of sample over extreme temperature ranges should not preclude its use. Z-meters do have a place in a serious thermoelectrics laboratory and as an instrument for quality control. This is especially true for research and development directed towards the improvement of a particular material where timely, relative measurements are important. Such measurements would be useful for many common thermoelectric materials for cooling and low temperature ($<700^{\circ}\text{C}$) generator applications.

A meter has been described which functions well on an absolute scale up to 300°C and on a relative scale up to 700°C . It employs a large temperature difference across the sample, which means that the results and the temperature stress on the sample reflect real-life situations. Data are not taken under thermal equilibrium conditions and the experimental design takes this into consideration. Key requirements for this type of meter are (1) the use of a computer to control the sequence of data collection, (2) a well-defined thermal geometry, and (3) a high signal-to-noise ratio in the thermometry and voltage probes. Many of the problems and solutions described will be common to any such meter.

References

1. Ioffe, A. F., *Semiconductor Thermocouples and Thermoelectric Cooling*, Infosearch Ltd., London, 1937, 38.
2. Putley, E. H., Thermoelectric and galvanomagnetic effects in lead selenide and telluride, *Proc. Phys. Soc. B (London)*, 68, 33, 1955.
3. Harman, T. C., Special techniques for measurement of thermoelectric properties, *J. Appl. Phys.*, 29, 1373, 1958; Harman, T. C., Cahn, J. H., and Logas, M. J., Measurement of thermal conductivity by utilization of the Peltier effect, *J. Appl. Phys.*, 30, 1351, 1959. (See also Kaganov, M. A., Linker, I. S., and Mushkin, I. G., On the problems of measuring thermoelectric properties of semiconductors, *Soviet Phys. Solid State*, 1, 905, 1959.
4. Linker, I. S., Determining an efficiency criterion for semiconductor materials, *Soviet Phys. Solid State*, 8, 1042, 1966.
5. See, e.g., Herlinsky, C. and Monfils, A., Electrical determination of the thermal parameters of semiconducting thermocouples, *Br. J. of Appl. Phys.*, 10, 235, 1959; Airey, Potts, S. V., Measurements of the thermoelectric properties of semiconductors at high temperatures by the Harman method in *Thermoelectric Properties of Semiconductors*, Kutasov, V. A., Ed., Consultants Bureau, New York 1964; Campbell, M. R. and Hogarth, C. A., A correction to the theory of Harman's method of determining the thermoelectric figure-of-merit, *International Journal of Electronics*, XIX, First Series

- 572, 1965; Al-Obaid, T. A. A. and Goldnerid, H. J., Determination of the thermoelectric figure-of-merit from thermal conductivity measurements, *Energy Conversion*, 9, 131, 1969; Efremov, A. A. and Pashkarskii, A. S., The measurement of the thermoelectric figure-of-merit of semiconductors in the presence of heat transfer at the junctions, *High Temp.-High Press.*, 2, 171, 1970; Trefny, J. U., Thin film characterizations using the Harman technique, *Proc. Fourth International Conference on Thermoelectric Energy Conversion*, University of Texas, Arlington, 1982, 79.
6. Phillips, L. S., The measurement of thermoelectric properties at high temperatures, *J. Sci. Instrum.*, 42, 289, 1965.
 7. Kaplan, M., Thermoelectric properties of rare earth chalcocrorites, *Proc. Fourth International Conference on Thermoelectric Energy Conversion*, University of Texas, Arlington, 1982, 37.
 8. Watanowicz, T. and Goscinski, M., Automatic measurement of thermoelectric material properties, *Proc. Seventh International Conference on Thermoelectric Energy Conversion*, University of Texas, Arlington, 1988, 156.
 9. Vedenikov, M. V., Konstantinov, P. P., and Il'nikov, A. T., Development of automated techniques of measuring the temperature dependences of the transport properties of thermoelectric materials, *Eighth International Conference on Thermoelectric Energy Conversion*, Nancy, 1989, 45.
 10. Van Winkleigh, R., Rapid simultaneous measurement of thermoelectric material properties, *Proc. Sixth International Conference on Thermoelectric Energy Conversion*, University of Texas, Arlington, 1986, 28. This paper provided the motivation for our own work but it is noted that it has serious methodological flaws.
 11. Yoshida, I. and Yunoki, I., Automatic measuring system of thermoelectric properties with a desktop computer, *Proc. Sixth International Conference on Thermoelectric Energy Conversion*, University of Texas, Arlington, 1986, 39.
 12. Woodbury, H. H., Lewandowski, R. S., Levinson, L. M., and Loughlin, S., A Z-Meter measurement on SiGe using a large-temperature-difference apparatus, *Proc. 12th International Conference on Thermoelectrics*, Pasadena, 1990, 303.
 13. Canack, N. and Kendall, F., The absolute scale of thermoelectric power at high temperature, *Proc. Phys. Soc. (London)*, 72, 898, 1958.
 14. Powell, R. W. et al., Thermal Conductivity of Selected Materials, National Standard Reference Data Systems, U.S. Department of Commerce, Washington, D.C., 25 November 1966. A least squares fit to the curves from 0°C to 700°C gives $k = 24.7 + 5456/(T + 334)$ mW/cm-sec where T is in C.
 15. Wu et al. have approached the problem of radial heat flow by measuring the temperature profile along hot and cold probes to a sample, and from this determining and correcting for heat loss in the sample. Wu, C. T., Lu, C. W., and Chou, D. J., The computer aided TE properties measurement system, *Proc. 12th International Conference on Thermoelectrics*, Pasadena, 1990, 312.
 16. Goldnerid, H. J. and Situmorang, M., Sintered bismuth telluride alloys — problems of orientation, *Eighth International Conference on Thermoelectric Energy Conversion*, Nancy, 1989, 1.